2019

GROWTH OF *SACCHARINA LATISSIMA* IN AQUACULTURE SYSTEMS MODELED USING DYNAMIC ENERGY BUDGET THEORY

Celeste T. Venolia
University of Rhode Island, celestevenolia@gmail.com

GROWTH OF *SACCHARINA LATISSIMA* IN AQUACULTURE SYSTEMS MODELED USING DYNAMIC ENERGY BUDGET THEORY

BY

CELESTE T. VENOLIA

A THESIS SUBMITTED IN PARTIAL FULFILLMENT OF THE

REQUIREMENTS FOR THE DEGREE OF

MASTER OF SCIENCE

IN

BIOLOGICAL AND ENVIRONMENTAL SCIENCES

UNIVERSITY OF RHODE ISLAND

2019

MASTER OF SCIENCE THESIS

OF

CELESTE T. VENOLIA

APPROVED:

Thesis Committee:

Major Professor Austin T. Humphries

Scott R. McWilliams

David S. Ullman

Nasser H. Zawia
DEAN OF THE GRADUATE SCHOOL

UNIVERSITY OF RHODE ISLAND
2019

ABSTRACT

Aquaculture is an industry with the capacity for further growth that can sustainably feed an increasing human population. Sugar kelp (*Saccharina latissima*) is of particular interest for farmers as a fast-growing species that benefits ecosystems. However, as a new industry in the U.S., farmers interested in growing *S. latissima* lack data on growth dynamics. To address this gap, we calibrated a Dynamic Energy Budget (DEB) model to data from the literature and a 2-year growth experiment in Rhode Island (U.S.). Environmental variables forcing model dynamics included temperature, irradiance, dissolved inorganic carbon (DIC) concentration, and nitrate and ammonium concentration. The modeled final estimate for *S. latissima* blade length (cm) was reasonably accurate despite underestimation of early season growth. Carbon limited winter growth due to a low modeled specific relaxation rate (i.e. the light-dependent reactions of photosynthesis) for some model runs; other model runs displayed nitrogen limitation which occasionally led to length overestimation and underestimation due to the degree of interpolation necessary from the field data. The model usage, however, is restricted to *S. latissima* grown in an aquaculture setting because of assumptions made about tissue loss, summer growth patterns, and reproduction. The results indicate that our mechanistic model for *S. latissima* captures growth dynamics and blade length at the time of harvest, thus it could be used for spatial predictions of kelp aquaculture production across a range of environmental conditions. The model could be a particularly useful tool for further development of sustainable ocean food production systems in the U.S. involving seaweed.

ACKNOWLEDGMENTS

A huge thank you to my advisor Austin Humphries for supporting me through these two years of work. Your calm and confident energy has always been a comfort though project challenges, and I admire the wide range of research you conduct though your work at URI. To my co-author Romain Lavaud, I cannot thank you enough for teaching me dynamic energy budget theory. The amount of time you have poured into answering my emails is greatly appreciated. Thank you to seaweed super-star Lindsay Green-Gavrielidis! I had an amazing time learning from you out in the field with the kelp. I would also like to acknowledge my committee members Dave Ullman and Scott McWilliams who both provided valuable critique and guidance. Thank you for all the time you spent teaching me how you work with Regional Ocean Modeling system, Dave! To the amazing folks in the Humphries lab past and present and affiliated (Lauren Josephs, Kelvin Gorospe, Evans Arizi, Elle Wibisono, Paul Carvalho, Elaine Shen, Annie Innes-Gold, Melati Kaye, Diana Beltran, Diky Suganda, Katie Viducic, Nicky Roberts and Catie Alves), thank you all for creating such a fun and supportive environment for group collaborative vibrations! Finally, love and thanks to my family whose continual support is what allowed me to go through this wild journey that is graduate school.

PREFACE

The following thesis has been submitted in manuscript format following the formatting guidelines of the journal *Ecological Modelling*.

TABLE OF CONTENTS

LIST OF TABLES

LIST OF FIGURES

FIGURE PAGE

CHAPTER 1

Modeling the Growth of Sugar Kelp (*Saccharina latissima*) in Aquaculture Systems using Dynamic Energy Budget Theory

Celeste T. Venolia[a], Romain Lavaud[b], Lindsay A. Green-Gavrielidis[c,d], Carol Thornber[c], and Austin Humphries[a,e*]

Manuscript in preparation for submission to the journal *Ecological Modelling*.

[a]Department of Fisheries, Animal and Veterinary Sciences, University of Rhode Island, Kingston, Rhode Island

[b]Institut des Sciences de la Mer, Université du Québec à Rimouski, Rimouski, QC, Canada

[c]Department of Natural Resources Science, University of Rhode Island, Kingston, Rhode Island

[d]*Present address:* Department of Biology and Biomedical Sciences, Salve Regina University, Newport, RI, USA

[e]Graduate School of Oceanography, University of Rhode Island, Narragansett, Rhode Island

* Corresponding Author.
Email Address: humphries@uri.edu (Austin Humphries)

Keywords
Rhode Island; food production; energetics; synthesizing units; seaweed

Abstract

Aquaculture is an industry with the capacity for further growth that can sustainably feed an increasing human population. Sugar kelp (*Saccharina latissima*) is of particular interest for farmers as a fast-growing species that benefits ecosystems. However, as a new industry in the U.S., farmers interested in growing *S. latissima* lack data on growth dynamics. To address this gap, we calibrated a Dynamic Energy Budget (DEB) model to data from the literature and a 2-year growth experiment in Rhode Island (U.S.). Environmental variables forcing model dynamics included temperature, irradiance, dissolved inorganic carbon (DIC) concentration, and nitrate and ammonium concentration. The modeled final estimate for *S. latissima* blade length (cm) was reasonably accurate despite underestimation of early season growth. Carbon limited winter growth due to a low modeled specific relaxation rate (i.e. the light-dependent reactions of photosynthesis) for some model runs; other model runs displayed nitrogen limitation which occasionally led to length overestimation and underestimation due to the degree of interpolation necessary from the field data. The model usage, however, is restricted to *S. latissima* grown in an aquaculture setting because of assumptions made about tissue loss, summer growth patterns, and reproduction. The results indicate that our mechanistic model for *S. latissima* captures growth dynamics and blade length at the time of harvest, thus it could be used for spatial predictions of kelp aquaculture production across a range of environmental conditions. The model could be a particularly useful tool for further development of sustainable ocean food production systems in the U.S. involving seaweed.

1. Introduction

With a growing global population, one of the greatest challenges is providing healthy diets from sustainable food systems (Duarte et al., 2009, Merino et al., 2012, Willett et al. 2019). Meeting these demands requires strategies for optimization and development across each food production industry in both terrestrial and aquatic habitats. Aquaculture is currently the fastest growing food production sector in the world and now produces more seafood than wild-capture fisheries (FAO, 2018). Within aquaculture, the ocean is increasingly viewed as an important area of expansion. This is because mariculture, or the farming of seafood in the ocean, has had one of the largest relative production increases in the last thirty years and has positive growth trajectories in many countries (Cottrell et al., 2018; Gentry et al., 2019). In fact, mariculture systems produced around 28.7 million tons of food in 2016 (FAO, 2018). The species, methods, and location of aquaculture will dictate its future contribution to the global food system within sustainable limits, particularly in the ocean (Gentry et al. 2017, Willett et al. 2019).

Aquaculture can have negative environmental impacts. In open systems of fed species, this negative impact is largely due to concentrated flows of feces and feed wastage leading to eutrophication (Wu, 1995) and alteration of food webs (Herbeck et al., 2013). Food for aquaculture species can put more pressure on terrestrial or aquatic food production systems, where the biomass harvested of one species is then reconstituted and serves as the input for the farming of another species (Cottrell et al., 2018). Open aquaculture systems composed of species that do not require supplemental feed or nutrients (i.e., primary producers and filter feeders) avoid these harms and instead can perform important ecosystem services such as removing

dissolved organic and inorganic nutrients (Alleway et al., 2019). In particular, seaweed is of interest for nutrient capture in integrated multi-trophic aquaculture (IMTA) systems where they utilize the inorganic carbon and nitrogenous compound outputs from fed species such as finfish (Chopin, 2015). Other potential benefits of growing seaweed are its ability to combat hypoxia from terrestrial food production systems and even protect shorelines through dampening of wave energy (Duarte et al., 2017). Outside of these ecosystem services, growing seaweed has been proposed as a way to engage a wider public audience with climate change via offsetting carbon emissions (Froehlich et al., 2019). Seaweed aquaculture has the potential to generate net positive environmental and social impacts, but this industry has been traditionally concentrated in Asian countries (FAO, 2018).

Seaweed aquaculture in the U.S. is a nascent industry. The U.S. does not produce enough aquatic plants to even register in the global production statistics (< 0.1%; FAO, 2018). In the Northeast U.S., sugar kelp (*Saccharina latissima*) is a local species of recent interest for food, biofuel, bioremediation, and pharmaceutical products (Forbord et al., 2012). *S. latissima* grows to large sizes very quickly and individuals can reach lengths greater than four meters in less than five years in the wild (Borum et al., 2002). In a single season of aquaculture growth, *S. latissima* blades can grow between 60-140 cm depending on the water depth, planting time, and nutrient availability (Handå et al., 2013). Oysters, however, are the most widely aquacultured species in coastal areas of the U.S (NMFS, 2018). The Eastern oyster (*Crassostrea virginica*) mostly grows during the summer months where water temperatures are above 15 °C and is in a state of relative dormancy in the winter

(Dame, 1972). Therefore, it has been suggested that *S. latissima* could complement farmed oysters because of the differences in growing season, thus providing an additional source of income without interfering with oyster production. This new industry, however, would benefit from production estimates that would enable farmers to decide whether it is possible or lucrative to farm kelp.

Bioenergetics allows for study of factors influencing an individual species' growth through assessment of energy relationships and transformations. Thus, bioenergetics models can support the creation of production estimates. Growth of *S. latissima* has been studied in both field and laboratory settings in response to environmental conditions. For example, the impacts of irradiance, temperature, and nutrient concentration on *S. latissima* growth were highlighted through a transplant experiment with kelps at different depths (Boden, 1979). In a simple predictive model created for *S. latissima*, growth was assumed to have a linear relationship with dissolved inorganic nitrogen concentration (with a temperature correction; Petrell et al., 1993). This model required an assumption that nitrogen dynamics are always limiting growth, thus ignoring the potential influence of irradiance. Light-harvesting characteristics of *S. latissima* have been shown to vary in populations from different ambient light regimes (Gerard, 1988), so irradiance is an important factor on this species' dynamics. Dynamic energy budget (DEB) theory provides a framework to examine the interactive effects of environmental nutrient concentrations and irradiance on an organism through parallel systems of nitrogen and carbon dynamics (Kooijman, 2010). DEB theory is a formal theory of metabolism, which is used to model the flow of mass and energy through an organism from uptake to usage for growth,

maintenance, reproduction, or excretion. DEB theory provides a sound mechanistic basis for understanding an organism's energetics.

Modeling autotrophs is a relatively new direction for DEB theory. The standard DEB model, which has been applied to many animal species, is appropriate for an animal that does not change shape through development and eats only one food source with a constant chemical composition. The standard DEB model has one reserve and one structure; structure and reserve are the central pools of matter modeled as state variables within an organism. For the application of DEB theory to autotrophs, such as *S. latissima*, multiple reserves are necessary to accurately model matter and energy dynamics because nutrient uptake can occur separately from photosynthesis (Kooijman, 2010). Autotroph DEB models have been constructed for microalgae (Lorena et al., 2010, Livanou et al., 2019), phytoplankton-zooplankton interactions (Poggiale et al., 2010), calcification of a coccolithophore (Muller and Nisbet, 2014), and the macroalga *Ulva lactuca* (Lavaud et al., under review). Other modelers have used dynamic bioenergetic models that borrow some concepts from DEB theory but selected a greater degree of simplification to model *S. latissima* (Broch and Slagstad, 2012) and the interaction between heterotrophic coral and autotrophic *Symbiodinium* spp. (Cunning et al., 2017). The model of Norwegian *S. latissima* was created as a tool for optimizing aquaculture production (Broch and Slagstad, 2012). They chose a simpler base structure than Lorena et al. (2010), but this simplification does not increase parsimony (i.e. reduce the number of model parameters) because of their use of correction functions where a DEB model would not need them. For example, a simple functional response is used to control the effect of frond size on gross growth

rate because smaller kelps grow faster than larger kelps (Broch and Slagstad, 2012). This would be redundant in a DEB model with maintenance because the maintenance cost is volume specific (Lorena et al., 2010).

Our primary objective is to develop a bioenergetics model for *S. latissima* growth. Specifically, we aim to calibrate the general structure of a macroalgae DEB model to our field data from Rhode Island (U.S.). The resulting model allows for growth predictions based on inputs of environmental conditions and has the potential to support the sustainable aquaculture industry, particularly with regard to site selection.

2. Methods

2.1 Dynamic Energy Budget Model Structure

The core structure of the *S. latissima* model tracked the uptake of carbon and nitrogen, their assimilation into reserves and allocation to growth, maintenance, or excretion (Figure 1). The variables that depict the state of the model were nitrogen reserve density, carbon reserve density, and structure. There were three differential equations to represent the change in the state variables over time. The differential equation solver used to run the model in R (R Core Team, 2019) was the package deSolve (Soetaert et al., 2010). The model initial conditions (Table S1a) and molecular weights for the structure and the reserves (Table S1b) were set at consistent values across each model run. The parameters (Table 1) and equations (Table 2) for this *S. latissima* model were based on Papadakis et al. (2005), Lorena et al. (2010), Livanou et al. (2019), and Lavaud et al. (under review). A detailed description of each model equation can be found in Appendix S2. An allometric relationship from Gevaert et al.

(2001) was used to convert from dry weight to the length of the kelp blade. This was a simplification from determining a shape coefficient which would be a more standard conversion factor in DEB theory. Finally, the model allowed for the prediction of kelp length, nutrient uptake, or rejection fluxes from data on irradiance, dissolved inorganic carbon (DIC) concentration, nitrate and ammonium concentration, and temperature.

2.2 Dynamic Energy Budget Model Assumptions

A core assumption of DEB theory, strong homeostasis, maintains that reserve and structure have constant chemical compositions (Kooijman, 2010). This does not mean that there are always constant amounts of reserve and structure; rather, it means that the amount of carbon, nitrogen, hydrogen, and oxygen relative to each other within specific reserves or structures remains constant. For example, laminarin and mannitol are key storage carbohydrates of *S. latissima* (Schiener et al., 2015). Therefore, we modeled the carbon reserves with a chemical composition similar to laminarin, mannitol, and glucose setting a constant ratio of one carbon to two hydrogen to one oxygen (1:2:1, C:H:O).

For our *S. latissima* DEB model, we considered two reserve pools: carbon and nitrogen (nitrate and ammonium, collectively); other potential nutrients such as phosphorous or potassium were dismissed. We feel this is a valid assumption, especially in regions where nitrogen is not abundant year-round and nitrogen availability is what drives accelerated growth in winter and early spring (Gagné et al., 1982). A previous dynamic model for Norwegian *S. latissima* growth also chose to use only a carbon and a nitrogen reserve (Broch and Slagstad, 2012). Adding further reserves to the model would increase complexity by increasing the number of state

variables and parameters with potentially little to no accompanying increase in accuracy. Our model also assumed that the energy carbon concentrating mechanisms used to convert bicarbonate into carbon dioxide do not have a significant impact on the overall energetics. The majority of the dissolved inorganic carbon in the ocean is in the form of bicarbonate (Raven et al., 2005); *S. latissima* and other algae use carbonic anhydrase in carbon concentrating mechanisms to assimilate bicarbonate and convert it into carbon dioxide (Axelsson et al., 2000). In other words, we assumed that assimilating carbon dioxide directly was identical to assimilating carbon dioxide that was formed extracellularly from bicarbonate through a carbon concentrating mechanism.

Another assumption of our DEB model was that *S. latissima* can be considered as a V1-morph. In DEB theory, V1-morphs are organisms whose surface area is proportional to volume, which simplifies the dynamics of the model (Kooijman, 2010). *Saccharina latissima* grows as a sheet in both length and width directions at the meristematic blade region near the stipe (Sjøtun, 1993). We were assuming variation in blade thickness over an individual blade and through time (Vettori and Nikora, 2017) would not have a substantial enough impact on this surface area to volume ratio to preclude the V-1 morph assumption. Assuming that surface area was proportional to volume is reasonable at sites where there are not major differences in water velocity. Drag from water speed has been found to change blade morphology; more sheltered environments have led to wider blades with ruffled edges and areas with strong currents have caused blades to be more strap-like (Buck and Buchholz, 2005). Even

with this plastic morphology, the change in blade height was still small enough to not significantly impact surface areas in regions with similar water speeds.

Other assumptions for this model were grounded in reducing the time of year that the model can be logically applied. Energy was not used for reproduction or maturity in our model for *S. latissima* as it would be in a standard DEB model, which is a simplification that allows for a more parsimonious model. *Saccharina latissima* peaks in reproduction twice a year, June and October, but can have reproductive tissue year-round (Lee and Brinkhuis, 1986). There is evidence it produces inhibitors that minimize the formation of reproductive tissue during the rapid growth phase (Buchholz and Lüning, 1999, Lüning et al., 2000). Reproductive development happens, but only for a small subset of blades by the time the aquaculture harvest occurs in Spring towards the end of first period of rapid growth. Apical frond loss in kelps is correlated with temperature stress and wave action (Krumhansl et al., 2014), mechanical stress of biofouling (Brown et al., 1997), and overall blade length (Sjøtun, 1993). Our model does not incorporate a correction for apical frond loss because we were focusing on the aquaculture season and the exact mechanism for this loss remains very context-specific in the literature. Furthermore, aquaculture farmers generally harvest kelp before biofouling begins, which maximizes harvestable blade length. We also assumed photoinhibition does not occur, which is similarly reasonable for the aquaculture season but not the summer. Photoinhibition does occur in *S. latissima* especially when high light conditions are combined with high temperature conditions (Heinrich et al., 2012). The aquaculture season of kelp is placed to maximize growth while minimizing loss or degradation of tissues due to various

stresses, and a tissue loss function would be necessary to accurately model wild kelp year-round.

2.3 Empirical Data

Saccharina latissima was grown at four oyster farm sites from fall to spring in both 2017-2018 and 2018-2019 (see Table S3 for exact plant and harvest dates). Kelp seed was raised in aquaria from harvested local reproductive kelp tissue collected at Ft. Wetherill, RI, following the methods of Redmond et al. (2014), and seed lines were attached to ropes held in place by moorings at each of the farms. The sites were split between Narragansett Bay and Pt. Judith Pond, RI (Figure 2). We placed duplicate longlines of kelp at a depth of 1-2 m at all the field sites. Kelp growth, measured as length and width (cm), was monitored every 20-85 days using a subset of individuals on the longline. The variability in monitoring timing was largely driven by the availability of farmers to assist with logistics as well as weather conditions.

Temperature data were collected every fifteen minutes using a HOBO® pendant logger. Water samples were collected when kelp growth measurements were taken to determine the concentrations of nitrate and ammonium. In 2017-2018, nitrate and ammonium concentration measurements were made using a LACHAT Flow Injection Autoanalyzer (LACHAT, 2008). In 2018-2019, nitrate and ammonium concentration measurements were made using an Astoria Pacific Model 303A Segmented Continuous Flow Autoanalyzer (Astoria-Pacific Inc, Clackamas, OR; Eaton et al., 1998).

2.4 Environmental Forcing Functions

The *S. latissima* model was forced with temperature, irradiance, dissolved inorganic carbon (DIC) concentration, and nitrate and ammonium concentration data on an hourly time step. Temperature recorded at fifteen-minute intervals were averaged on an hourly basis and was identical at each kelp line at a specific site and year in the model because we only had a logger on one of the longlines at each site and assumed the conditions were the same at the other. Due to difficulties with biofouling on irradiance loggers, we used radiative forcing from the North American Regional Reanalysis (Mesinger et al., 2006) to estimate photosynthetically active radiation (PAR; Appendix S4). We used linear interpolation to create an hourly forcing from source data from every three hours (Figure 3). All sites have the same base irradiance forcing in one year using this method. DIC concentration data were not collected in this study, so this forcing is estimated from other sources. The Pt. Judith Pond sites were held at a constant DIC value based on U.S. Environmental Protection Agency data from Ninigret Pond (J. Grear, unpublished data). The Narragansett Bay sites were held at a constant DIC value based on data from Brenton Point (Segarra, 2002). We used linear interpolation to estimate hourly nitrate and ammonium concentrations.

2.5 Model Calibration

The parameters for our model were set using a combination of manual fitting to literature data, values from previous autotroph DEB models, and field data from this study (Table 1). Literature data on basic physiological rates were compiled to simultaneously calibrate parameters using the model equations (Table 3). Information about the locations where these studies were conducted was also included because

there are multiple ecotypes of *S. latissima* (Gerard, 1988), which may influence their physiological response. Due to a lack of local information on certain aspects of kelp growth, this model was calibrated with data across multiple ecotypes of kelp. The Arrhenius relationship parameters were calculated using a least squared non-linear regression on the compiled literature rates which were standardized using the reference temperature. The nitrate and ammonium uptake parameters, maximum volume specific nitrogen assimilation and half-saturation concentration for NO_3^- and NH_4^+ uptake, were calibrated using nitrate uptake data from Espinoza and Chapman (1983). Photosynthesis parameters, photosynthetic unit (PSU) density, binding probability of a photon to a free light synthesizing unit, and dissociation rate of releasing ATP and $NADPH^+$, were calibrated using oxygen production data from Johansson and Snoeijs (2002). Root mean square error (RMSE) was used as a measure of spread in the residuals for assessing the quality of each parameter calibration.

2.6 Sensitivity Analyses

To determine how each DEB parameter influenced results, we analyzed the local sensitivity of $\boldsymbol{m_{E_C}}$ C reserve density, $\boldsymbol{m_{E_N}}$ N reserve density, and $\boldsymbol{M_V}$ structural mass to model parameters using an L1 summary value of sensitivity from the R package FME (Soetaert and Petzoldt, 2010). L1 is a summation of the absolute value of all the elements in a sensitivity matrix divided by the number of elements. Each element of the sensitivity matrix is calculated by multiplying the change in the output variable over the change in a parameter to the scaling of that same parameter over the scaling of that same output variable. The scaling here is usually equal to the value of the variable or parameter (Soetaert and Petzoldt, 2010). Parameters have unequal

impacts on model outcomes, and this method allowed us to determine what parameters are having the largest effects on $\boldsymbol{m_{E_C}}$, $\boldsymbol{m_{E_N}}$, and $\boldsymbol{M_V}$.

3. Results

3.1 Model Calibration: Literature Data

The Arrhenius relationship fit to the compiled literature data (Table 3) reflected maximum physiological rates at temperatures around 13 °C (Figure 4). The lower boundary of the Arrhenius relationship was 0 °C, and the upper boundary was 13.39 °C. The adjusted R-squared for this relationship was 0.55 (p-value = 2.74e-11).

Using the nitrate uptake data from Espinoza and Chapman's (1983) site that was seasonally depleted of nitrate between April and November provided estimates of maximum volume specific ammonium and nitrate assimilation of 2.7 $*10^{-4}$ (mol N mol M_V^{-1} h^{-1}) and a half-saturation concentration of 2.667 $*10^{-6}$ (mol NO_3^- and NH_4^+ L^{-1}) (Figure 5). The fit for the data collected at 18 °C was slightly better at a RMSE of 9.73e-07 (mol N gDW^{-1} h^{-1}) than the 9 °C data at 1.43e-06 (mol N gDW^{-1} h^{-1}).

For the oxygen production data (Johansson and Snoeijs, 2002) used to calibrate the photosynthesis parameters, the values that had the lowest error around the data were a ρ_{PSU} photosynthetic unit (PSU) density of 0.05 (mol PSU mol M_V^{-1}), a $\dot{b}_I$ binding probability of a photon to a free light synthesizing unit of 2.8 $*10^{-6}$ (unitless), and a $\dot{k}_I$ dissociation rate of releasing ATP and $NADPH^+$ of 0.28 (mol NADPH mol PSU^{-1} h^{-1}; Figure 6). The resulting RMSE was 0.000457 (g O_2 g DW^{-1} h^{-1}). The maximum oxygen production rate of the model was around 0.00495 g O_2 g DW^{-1} h^{-1} (Figure 6).

Appropriate literature data for calibrating carbon dioxide uptake were not available. Air-based carbon dioxide uptake data for *S. latissima* (Ní Longphuirt et al.,

2013) were examined but ultimately rejected due to likely dissimilarity to submerged carbon dioxide uptake. Other parameters in DEB models such as the reserve turnover rates could not be compared to measurable physiological data due to the internal nature of the processes without easily interpretable signals, so these parameters were set at values similar to those in Lorena et al. (2010) and Lavaud et al. (under review).

3.2 Model Forcing Functions: Field Data

Converting the collected environmental field data into hourly values involved varying degrees of estimation which result in diverging degrees of accuracy. The temperature correction functions for both kelp growth seasons showed a seasonal trend and were the most accurate of the forcing information because the loggers were reliable and collected data on fifteen-minute intervals (Figure 7). For 2017-2018, the maximum water temperature recorded at our sites was 16.7 °C in November resulting in a temperature correction of 1.27 and the minimum temperature was -1.72 °C in January resulting in a temperature correction of 0.48. For 2018-2019, the maximum ocean temperature was 15.28 °C in May resulting in a temperature correction of 1.35 and the minimum temperature was -1 °C in January resulting in a temperature correction of 0.52. For comparison, the temperature at which maximum physiological rates occur (13°C) had a 1.4 temperature correction. Temperature changes were consistent across all four sites for both years.

The nitrate and ammonium concentration forcing variable had larger inaccuracy than temperature because of the linear extrapolation between the measurements (Figure 8). The mean nitrogen concentration at the Pt. Judith Pond sites was 4.37e-06 mol NO_3^- and NH_4^+ L^{-1} (± 3.69e-06) and 1.32e-06 mol NO_3^- and NH_4^+ L^{-1} (± 3.21e-06) at the Narragansett Bay sites for 2017-2018. For 2018-2019, the mean

nitrogen concentration at the Pt. Judith Pond sites was 2.19e-06 mol NO_3^- and NH_4^+ L^{-1} (± 2.28e-06) and 4.07e-06 mol NO_3^- and NH_4^+ L^{-1} (± 4.38e-06) at the Narragansett Bay sites.

The maximum PAR estimated in the irradiance forcing was 3,833,408 μE m^{-2} h^{-1} in 2017-2018 on the last day of harvest (4/22/18) and 3,977,676 μE m^{-2} h^{-1} in 2018-2019 close to the harvest in Narragansett Bay (5/22/19) (Figure 3).

3.3 *S. latissima* Growth and Model Dynamics

Saccharina latissima grew quickly with mean elongation across all sites studied of 0.87 ± 0.63 cm/d in 2017-2018 and 1.18 ± 0.62 cm/d in 2018-2019 (Figure 9). End of season blade length growth varied, but no clear site variation was observed (Table 4). The *S. latissima* DEB model generally underestimated growth observed in the early parts of the season (planting to end of March) but accurately predicted the length at harvest within one standard deviation of the observed mean length for some sites (Figure 9 and 10). An exception to this trend was the first kelp line planted at Pt. Judith Pond South in the 2017-2018 growing season for which length was overestimated by the end of the season. The RMSEs for the model length prediction to the field length data ranged widely from 5.16 to 62.72 cm (Figure 9).

Examining internal model dynamics allowed for clearer understanding of predicted growth. Specifically, examining the reject fluxes (mass rejected at the growth synthesizing unit based on the stoichiometric ratio of C or N reserve compounds required for building structure) allowed for examination of model limitation. The side of the model (C or N) with a flatline or decreasing trend in the reject flux is the side limiting growth. The carbon reserve (carbohydrates) limited model growth after planting for greatly variable timespans across the sites, seasons,

and lines (Figure S5a, Figure 5b). For example, in Pt Judith Pond in 2018-2019, at the S site, the C reserve is essentially never limiting due to persistent N reserve limitation whereas, at the N site, carbon limitation persists until March (Figure S5a and S5b). N is generally limiting by the end of the kelp aquaculture season (Figure S5a and S5b). Since both irradiance and DIC concentration impact carbon assimilation, plots of these initial assimilation fluxes revealed which one of these factors limits carbon assimilation. The specific assimilation rate of carbon mirrored the shape of the specific relaxation rate (Figure S5c and S5d). The shape of the specific relaxation rate (Figure S5c) reflected the influence of the temperature correction (Figure 7) rather than that of the magnitude of the irradiance forcing (Figure 3).

3.4 Sensitivity Analyses

The parameters with the largest effects (>3000 L1 summary value of sensitivity functions) on the state variables were $\boldsymbol{m_{E_C}}$ C reserve density, $\boldsymbol{m_{E_N}}$ N reserve density, and $\boldsymbol{M_V}$ structural mass were $\boldsymbol{T_0}$ reference temperature, $\boldsymbol{T_H}$ upper boundary of temperature tolerance, $\boldsymbol{T_L}$ lower boundary of temperature tolerance, $\boldsymbol{T_{AH}}$ Arrhenius temperature outside T_H, $\boldsymbol{T_{AL}}$ Arrhenius temperature outside T_L, $\boldsymbol{y_{E_CV}}$ yield factor of C reserve to structure, $\boldsymbol{\kappa_{E_i}}$ fraction of rejection flux incorporated back in i-reserve, $\boldsymbol{y_{IC}}$ yield factor of C reserve to NADPH, and $\boldsymbol{y_{CO_2C}}$ yield factor of C reserve to CO_2 (Figure 11). The parameters with the moderate effects (1000-2000) on the state variables were $\dot{\boldsymbol{J}}_{\boldsymbol{E_CAm}}$ max. volume specific carbon assimilation, and $\dot{\boldsymbol{k}}_{\boldsymbol{I}}$ dissociation rate of releasing ATP and $NADPH^+$. The parameters with small but non-zero effects on the state variables were $\boldsymbol{y_{E_NV}}$ yield factor of N reserve to structure, $\dot{\boldsymbol{k}}_{\boldsymbol{EC}}$ carbon reserve turnover rate, and $\boldsymbol{\rho_{PSU}}$ photosynthetic unit (PSU) density (Figure 11).

4. Discussion

Further mariculture development represents a key role in expanding U.S. sustainable food production, and macroalgae can provide high returns if the proper growth conditions exist. Thus, understanding the growth dynamics of *S. latissima* can provide the industry with a powerful predictive tool for estimating production. Our model is the first attempt to apply Dynamic Energy Budget (DEB) theory to a macroalga of the order Laminariales. The model tended to underestimate initial growth of *S. latissima* due to a low modeled specific relaxation rate or for sites where N was limiting an inaccurate N forcing. The model was good, however, at predicting final growth rates (Figure 10). Our process-based model also allowed us to better understand local growth limitations as they relate to the behavior of the model.

4.1 Growth Limitation

We hypothesize that the early season model underestimation of *S. latissima* length growth results from limited modeled carbon assimilation due to a low modeled specific relaxation rate (i.e. the light-dependent reactions of photosynthesis) for those model runs where C dynamics are the limiting factor. Seasonal temperature change and diurnal irradiance oscillation appear to control C assimilation via the specific relaxation rate rather than a seasonal trend of irradiance magnitude change. There is some evidence that winter limitation of C dynamics occurs in the field; *S. latissima* individuals older than a year were shown to have a decrease in blade C content mid-winter suggesting consumption of stored carbohydrates (Sjøtun, 1993). New sporophytes would not have this carbohydrate pool to draw upon. This decrease in C content suggests that C dynamics may be limiting *S. latissima* growth, but limitation was not directly examined by Sjøtun (1993).

For those model runs where C dynamics are the limiting factor, the early season (planting to end of March) model underestimation of field growth may reflect that the temperature correction has too powerful of an impact on the specific relaxation rate in comparison to irradiance. The seasonal trend of the specific relaxation rate reflects the seasonality of temperature; we suspect that the assumption of temperature impacting $\dot{k}_I$ dissociation rate of releasing ATP and $NADPH^+$ may cause temperature to have an outsized impact in comparison to irradiance magnitude. Ocean temperature trends trail behind irradiance change, and Narragansett Bay is no exception to this pattern (Brady-Campbell et al., 1984). *Saccharina latissima*'s early season growth could be driven by this early season increase in irradiance rather than water temperature change. This possibility is further reason to verify an organism's Arrhenius relationship regionally if there is potential for different degrees of temperature adaptation. More data is necessary to confirm if the *S. latissima* model underestimates winter kelp growth due to the impact of temperature on modeled photosynthesis.

Other than an increase in irradiance, daylength is a linked variable that could impact seasonal growth patterns. Broch and Slagstad's (2012) *S. latissima* model used the rate of change of day length in a photoperiodic effect function to create seasonality in their growth prediction. This is based on the hypothesis that *S. latissima* is a "seasonal anticipator" with endogenous circadian rhythms (Kain, 1989). Seasonal anticipators are posited to grow strategically in response to a trigger as opposed to simply responding to environmental conditions. Other kelps, *Laminaria hyperborea* and *Laminaria digitata*, have been shown to have free-running seasonal growth

patterns which suggests control by endogenous circadian rhythms (Schaffelke and Lüning, 1994). Species-specific evidence for this circadian hypothesis is lacking including the mechanism for what would trigger *S. latissima*'s photoperiodic response.

Another possible reason for underestimation of early season carbon dynamics in the *S. latissima* model may be a lack of energy gain at night. *Saccharina latissima*'s carbon dioxide exchange rate, the difference in inflow and outflow carbon dioxide multiplied by the airflow rate, is not closely correlated with irradiance because carbon dioxide uptake by the alga continues into the dark (Mortensen, 2017). Light-independent carbon fixation relies on energy from the light reactions during the day (Cabello-Pasini and Alberte, 2001). On average, 11% of *S. latissima*'s carbon fixation happens in the dark (Kremer and Markham, 1979). The linkage between the light-dependent and light-independent reactions is modeled as an immediate transference. In other words, when there is no irradiance input to the *S. latissima* model, the assimilation of carbohydrates to the carbon reserve is zero. This is not reflective of the lag which allows for the formation of carbohydrates in the dark, but we would argue that adding this layer of physiological accuracy would reduce model efficiency without enough increase in the predictive capacity.

Where N dynamics limit growth below the level observed in the field, the heavily interpolated N forcing is likely not reflective of actual conditions. The N forcing effects our ability to fit the overall model tightly to all runs simultaneously due to overestimation of blade length in some runs with an overinflated N forcing and underestimation in others.

4.2 Sensitivity Analysis

Identifying parameters that a model is highly sensitive to gives us a clearer idea of what parameters are likely to shift the overall fit of a model (Soetaert and Petzoldt, 2010). The high sensitivity of the state variables to the temperature related parameters is a logical outcome of the central role of temperature in DEB theory. Since the temperature correction is applied to such a large number of rates in the organism, the high sensitivity to these values is reasonable. The sensitivity of the model to the temperature parameters is an argument for caution in regional calibration of the Arrhenius relationship. The sensitivity of the kelp model to $\boldsymbol{\kappa_{E_i}}$ fraction of rejection flux incorporated back in i-reserve contrasts with the sensitivity of Lorena et al (2010)'s microalgae model to the same parameter. The fact that the kelp model is sensitive to changes in $\boldsymbol{\kappa_{E_i}}$ is concerning as this is not a parameter that we can easily determine with relevant literature data. $\boldsymbol{y_{IC}}$ yield factor of C reserve to NADPH and $\boldsymbol{y_{CO_2C}}$ yield factor of C reserve to CO_2 are parameters that the model is highly sensitive to which reflects their divisor positions in specific assimilation rate of C equation; these are not important parameters to focus on because their values reflect ratios laid out by the photosynthesis equations, so they would not be modified to adjust model fit. The high sensitivity of the kelp model to $\boldsymbol{y_{E_CV}}$ yield factor of C reserve to structure in comparison to the small but nonzero impact of $\boldsymbol{y_{E_NV}}$ yield factor of N reserve to structure might be reflective of the relative proportions greater amount of C reserve required by the chemical composition of the structure. This concept is similarly supported by the majority of the parameters the state variables are sensitive to being a part of C dynamics such as the moderate sensitivity to $\boldsymbol{\dot{J}_{E_CAm}}$ maximum

volume specific carbon assimilation and $\dot{k}_I$ dissociation rate of releasing ATP and $NADPH^+$. The state variables are more sensitive to $\dot{k}_I$ than the other photosynthesis parameters which likely reflects its position of power as a divisor in the specific relaxation rate equation.

4.3 Model Application

Limitations to broader geographic use of this model center around the plasticity of *S. latissima* and the existence of ecotypes. The differentiation of ecotypes occurs when individuals have an acclimation range related to their habitat of origin (Gerard, 1988). For instance, *S. latissima* individuals from New York have been shown to have a different physiological response to temperature in a lab setting than individuals from Maine (Gerard, 1988). Narragansett Bay, RI is located towards the southern boundary of where *S. latissima* can survive (Taylor, 1972). The existence of multiple ecotypes of this species suggests that parameters may require regional adjustment, particularly in the Arctic. Our model assumptions about surface area's proportionality to volume impedes prediction of blade shape plasticity, which is a characteristic of *S. latissima* related to drag (Buck and Buchholz, 2005). Since the blade thickness and amount of blade ruffling impact the relationship between surface area and volume, this complicates the use of the model in areas with either significantly different amounts of drag from water motion or highly variable water motion.

Further research on the mechanisms for frond loss, blade plasticity, and regional parameter information have the potential to improve this DEB model. A clearer physiological cause for apical frond loss would allow this to be included in mechanistic models in a more meaningful way than a correction function setting

erosion based on one correlated variable like length or age. Similarly, determining a mechanism for how blade type changes in response to variable water speeds would provide a clearer picture of overall growth dynamics. Other data that would be useful for understanding *S. latissima* physiology and increasing the accuracy of predictive modeling are underwater carbon dioxide uptake data in response to variable irradiance and more regionally appropriate oxygen production data in response to variable irradiance.

Our *S. latissima* model is a first step towards estimating kelp aquaculture production in the U.S. Norwegian *S. latissima* research highlights the potential of dynamic modeling to both estimate the effectiveness of *S. latissima* as a nutrient assimilator in integrated multi-trophic aquaculture (IMTA) systems (Broch et al., 2013, Fossberg et al., 2018) and estimate aquaculture production at large scales using a coupled biogeochemical-hydrodynamic-kelp model (Broch et al., 2019). In future work, our *S. latissima* DEB model could be coupled with a DEB model for *C. virginica* (Filgueira et al., 2014; Lavaud et al., 2017) and the Regional Ocean Modeling System (ROMS) with a Carbon Silicate Nitrogen Ecosystem (CoSiNE) model (Chai et al, 2009) to predict growth potential at sites. ROMS is a widely-used primitive equations ocean model and the CoSINE model integrates biogeochemical processes (Chai et al, 2009). Running a biogeochemical-hydrodynamic model would allow for farm scale predictions of environmental conditions, such as nutrients and light, that impact kelp growth. Mixed-methods modeling, such a DEB-ROMS coupling, can support logical expansion of coastal aquaculture.

5. Acknowledgements

Thank you to Cindy and John West of Cedar Island Oysters, Russ Blank and Thomas of Rome Point Oyster Farm, and Trip Whilden of Wickford Oyster Co for working with us to grow kelp for two years. Dave Ullman and Chris Kincaid for their role in the initial project development. Thomas Guyondet for facilitating collaborations around this project. Marine Science Research Facility at GSO and Kelly Addy for water analysis. T. Ben-Horin for assistance collecting reproductive kelp. J. Barnes, A. Barry, R. Derouin, E. Ferrante, I. Gray, K. Hannibal, C. Jenkins, A. Mauk, L. Sebesta, A. Wetzel for lab and field help. S. McWilliams, D. Ullman, M. Gomez-Chiarri, L. Josephs, and K. Gorospe for feedback.

Funding: This work is supported by the National Oceanic and Atmospheric Administration Saltonstall-Kennedy grant [17GAR008] and NSERC grant [497065-2016].

6. References

Alleway, H. K., Gillies, C. L., Bishop, M. J., Gentry, R. R., Theuerkauf, S. J., & Jones, R. (2019). The ecosystem services of marine aquaculture: Valuing benefits to people and nature. *BioScience*, *69*(1), 59-68.

Axelsson, L., Mercado, J., & Figueroa, F. (2000). Utilization of HCO_3^- at high pH by the brown macroalga *Laminaria saccharina*. *European Journal of Phycology*, *35*(1), 53-59.

Boden, G. T. (1979). The effect of depth on summer growth of *Laminaria saccharina* (Phaeophyta, Laminariales). *Phycologia*, *18*(4), 405-408.

Bolton, J. J., & Lüning, K. (1982). Optimal growth and maximal survival temperatures of Atlantic *Laminaria* species (Phaeophyta) in culture. *Marine Biology*, *66*(1), 89-94.

Borum, J., Pedersen, M., Krause-Jensen, D., Christensen, P., & Nielsen, K. (2002). Biomass, photosynthesis and growth of *Laminaria saccharina* in a high-arctic fjord, NE Greenland. *Marine Biology*, *141*(1), 11-19.

Brady-Campbell, M. M., Campbell, D. B., & Harlin, M. M. (1984). Productivity of kelp (*Laminaria* spp.) near the southern limit in the northwestern Atlantic Ocean. *Marine Ecology Progress Series*, *18*(1), 79-88.

Broch, O. J., & Slagstad, D. (2012). Modelling seasonal growth and composition of the kelp *Saccharina latissima*. *Journal of Applied Phycology*, *24*(4), 759-776.

Broch, O. J., Ellingsen, I. H., Forbord, S., Wang, X., Volent, Z., Alver, M. O., ... & Olsen, Y. (2013). Modelling the cultivation and bioremediation potential of the kelp *Saccharina latissima* in close proximity to an exposed salmon farm in Norway. *Aquaculture Environment Interactions*, *4*(2), 187-206.

Broch, O. J., Alver, M. O., Bekkby, T., Gundersen, H., Forbord, S., Handå, A., ... & Hancke, K. (2019). The kelp cultivation potential in coastal and offshore regions of Norway. *Frontiers in Marine Science*, *5*, 529.

Brown, M. T., Nyman, M. A., Keogh, J. A., & Chin, N. K. M. (1997). Seasonal growth of the giant kelp *Macrocystis pyrifera* in New Zealand. *Marine Biology*, *129*(3), 417-424.

Buchholz, C., & Lüning, K. (1999). Isolated, distal blade discs of the brown alga *Laminaria digitata* form sorus, but not discs, near to the meristematic transition zone. *Journal of Applied Phycology*, *11*(6), 579.

Buck, B. H., & Buchholz, C. M. (2005). Response of offshore cultivated *Laminaria saccharina* to hydrodynamic forcing in the North Sea. *Aquaculture*, *250*(3-4), 674-691.

Cabello-Pasini, A., & Alberte, R. S. (2001). Expression of carboxylating enzymes in *Laminaria setchellii* (Phaeophyceae). *Phycologia*, *40*(4), 351-358.

Chai, F., G. Liu, H. Xue, L. Shi, Y. Chao, C.-M. Tseng, W.-C. Chou, and K.-K. Liu (2009). Seasonal and interannual variability of carbon cycle in South China Sea: A three-dimensional physical-biogeochemical modeling study, *Journal of Oceanography,* 65, 703-720.

Chopin, T. (2015). Marine aquaculture in Canada: well-established monocultures of finfish and shellfish and an emerging Integrated Multi-Trophic Aquaculture (IMTA) approach including seaweeds, other invertebrates, and microbial communities. *Fisheries*, *40*(1), 28-31.

Cottrell, R. S., Fleming, A., Fulton, E. A., Nash, K. L., Watson, R. A., & Blanchard, J. L. (2018). Considering land–sea interactions and trade-offs for food and biodiversity. *Global change biology*, *24*(2), 580-596.

Cunning, R., Muller, E. B., Gates, R. D., & Nisbet, R. M. (2017). A dynamic bioenergetic model for coral-*Symbiodinium* symbioses and coral bleaching as an alternate stable state. *Journal of Theoretical Biology*, *431*, 49-62.

Dame, R. F. (1972). The ecological energies of growth, respiration and assimilation in the intertidal American oyster *Crassostrea virginica*. *Marine biology*, *17*(3), 243-250.

Davison, I. R. (1987). Adaptation of photosynthesis in *Laminaria saccharina* (Phaeophyta) to changes in growth temperature. *Journal of Phycology*, *23*, 273-283.

Davison, I. R., & Davison, J. O. (1987). The effect of growth temperature on enzyme activities in the brown alga *Laminaria saccharina*. *British Phycological Journal*, *22*(1), 77-87.

Duarte, C. M., Holmer, M., Olsen, Y., Soto, D., Marbà, N., Guiu, J., Black, K., & Karakassis, I. (2009). Will the oceans help feed humanity? *BioScience*, *59*(11), 967-976.

Duarte, C. M., Wu, J., Xiao, X., Bruhn, A., & Krause-Jensen, D. (2017). Can seaweed farming play a role in climate change mitigation and adaptation? *Frontiers in Marine Science*, *4*, 100.

Eaton, A. D., Clesceri L. S., Greenberg A. E., & Franson M. H. (1998) Standard methods for the examination of water and wastewater. APHA, AWWA, and WEF, Washington, DC.

Espinoza, J., & Chapman, A. R. O. (1983). Ecotypic differentiation of *Laminaria longicruris* in relation to seawater nitrate concentration. *Marine Biology*, 74(2), 213-218.

FAO. 2018. *The State of World Fisheries and Aquaculture 2018 - Meeting the sustainable development goals.* Rome. Licence: CC BY-NC-SA 3.0 IGO.

Filgueira, R., Guyondet, T., Comeau, L. A., & Grant, J. (2014). A fully-spatial ecosystem-DEB model of oyster (*Crassostrea virginica*) carrying capacity in the Richibucto Estuary, Eastern Canada. *Journal of Marine Systems*, *136*, 42-54.

Forbord, S., Skjermo, J., Arff, J., Handå, A., Reitan, K. I., Bjerregaard, R., & Lüning, K. (2012). Development of *Saccharina latissima* (Phaeophyceae) kelp hatcheries with year-round production of zoospores and juvenile sporophytes on culture ropes for kelp aquaculture. *Journal of Applied Phycology*, *24*(3), 393-399.

Fortes, M. D., & Lüning, K. (1980). Growth rates of North Sea macroalgae in relation to temperature, irradiance and photoperiod. *Helgoländer Meeresuntersuchungen*, *34*(1), 15.

Fossberg, J., Forbord, S., Broch, O. J., Malzahn, A. M., Jansen, H., Handa, A., ... & Olsen, Y. (2018). The potential for upscaling kelp (*Saccharina latissima*) cultivation in salmon-driven integrated multi-trophic aquaculture (IMTA). *Frontiers in Marine Science*, *5*, 418.

Froehlich, H. E., Afflerbach, J. C., Frazier, M., & Halpern, B. S. (2019). Blue Growth Potential to Mitigate Climate Change through Seaweed Offsetting. *Current Biology*, 29, 1-7.

Gagné, J. A., Mann, K. H., & Chapman, A. R. O. (1982). Seasonal patterns of growth and storage in *Laminaria longicruris* in relation to differing patterns of availability of nitrogen in the water. *Marine Biology*, *69*(1), 91-101.

Gentry, R. R., Froehlich, H. E., Grimm, D., Kareiva, P., Parke, M., Rust, M., ... & Halpern, B. S. (2017). Mapping the global potential for marine aquaculture. *Nature Ecology & Evolution*, *1*(9), 1317-1324.

Gentry, R. R., Ruff, E. O., & Lester, S. E. (2019). Temporal patterns of adoption of mariculture innovation globally. *Nature Sustainability*, *2*(10), 949-956.

Gevaert, F., Davoult, D., Creach, A., Kling, R., Janquin, M. A., Seuront, L., & Lemoine, Y. (2001). Carbon and nitrogen content of *Laminaria saccharina* in the eastern English Channel: biometrics and seasonal variations. *Journal of the Marine Biological Association of the United Kingdom*, *81*(5), 727-734.

Gerard, V. A. (1988). Ecotypic differentiation in light-related traits of the kelp *Laminaria saccharina*. *Marine Biology*, *97*(1), 25-36.

Handå, A., Forbord, S., Wang, X., Broch, O. J., Dahle, S. W., Størseth, T. R., ... & Skjermo, J. (2013). Seasonal-and depth-dependent growth of cultivated kelp (*Saccharina latissima*) in close proximity to salmon (*Salmo salar*) aquaculture in Norway. *Aquaculture*, *414*, 191-201.

Heinrich, S., Valentin, K., Frickenhaus, S., John, U., & Wiencke, C. (2012). Transcriptomic analysis of acclimation to temperature and light stress in *Saccharina latissima* (Phaeophyceae). *PLoS One*, *7*(8), e44342.

Herbeck, L.S., Unger, D., Wu, Y., & Jennerjahn, T.C., (2013). Effluent, nutrient and organic matter export from shrimp and fish ponds causing eutrophication in coastal and back-reef waters of NE Hainan, tropical China. *Continental Shelf Research* 57, 92–104.

Johansson, G., & Snoeijs, P. (2002). Macroalgal photosynthetic responses to light in relation to thallus morphology and depth zonation. *Marine Ecology Progress Series*, *244*, 63-72.

Kain, J. M. (1989). The seasons in the subtidal. *British Phycological Journal*, *24*(3), 203-215.

Kooijman, S. A. L. M. (2010). *Dynamic energy budget theory for metabolic organisation*. Cambridge university press.

Kremer, B. P., & Markham, J. W. (1979). Carbon assimilation by different developmental stages of *Laminaria saccharina*. *Planta*, *144*(5), 497-501.

Krumhansl, K. A., Lauzon-Guay, J. S., & Scheibling, R. E. (2014). Modeling effects of climate change and phase shifts on detrital production of a kelp bed. *Ecology*, *95*(3), 763-774.

LACHAT (2008). QuikChem Method 31-107-04-1-A. LACHAT INSTRUMENTS, Loveland, CO.

LACHAT (2008). QuikChem Method 31-107-06-1-B. LACHAT INSTRUMENTS, Loveland, CO.

Lavaud, R., La Peyre, M. K., Casas, S. M., Bacher, C., & La Peyre, J. F. (2017). Integrating the effects of salinity on the physiology of the eastern oyster, *Crassostrea virginica*, in the northern Gulf of Mexico through a Dynamic Energy Budget model. *Ecological Modelling*, *363*, 221-233.

Lavaud, R., Filgueira, R., Nadeau, A., Steeves, L., & Guyondet, T. (under review). A Dynamic Energy Budget model for the macroalga *Ulva lactuca*. *Ecological modelling*.

Lee, J. A., & Brinkhuis, B. H. (1986). Reproductive phenology of *Laminaria Saccharina* (L.) Lamour. (Phaeophyta) at the Southern limit of its distribution in the Northwestern Atlantic Ocean. *Journal of Phycology*, *22*(3), 276-285.

Livanou, E., Lagaria, A., Psarra, S., & Lika, K. (2019). A DEB-based approach of modeling dissolved organic matter release by phytoplankton. *Journal of sea research*, *143*, 140-151.

Lorena, A., Marques, G. M., Kooijman, S. A. L. M., & Sousa, T. (2010). Stylized facts in microalgal growth: interpretation in a dynamic energy budget context. *Philosophical Transactions of the Royal Society B: Biological Sciences*, *365*(1557), 3509-3521.

Lüning, K., Wagner, A., & Buchholz, C. (2000). Evidence for inhibitors of sporangium formation in *Laminaria digitata* (Phaeophyceae) during the season of rapid growth. *Journal of Phycology*, *36*(6), 1129-1134.

Merino, G., Barange, M., Blanchard, J. L., Harle, J., Holmes, R., Allen, I., Allison, E.H., Badjeck, M.C., Dulvy, N.K., Holt, J., & Jennings, S. (2012). Can marine fisheries and aquaculture meet fish demand from a growing human population in a changing climate? *Global Environmental Change*, *22*(4), 795-806.

Mesinger, F., G. DiMego, E. Kalnay, K. Mitchell, and Coauthors, 2006: North American Regional Reanalysis. *Bulletin of the American Meteorological Society*, **87**, 343–360.

Mortensen, L. M. (2017). Diurnal carbon dioxide exchange rates of *Saccharina latissima* and *Laminaria digitata* as affected by salinity levels in Norwegian fjords. *Journal of Applied Phycology*, *29*(6), 3067-3075.

Mõttus, Matti & Sulev, Madis & Frederic, Baret & Lopez-Lozano, R. & Reinart, Anu. (2011). Photosynthetically Active Radiation: Measurement and Modeling. In R.

Meyers (Ed.), *Encyclopedia of Sustainability Science and Technology* (pp. 7970-8000). New York, NY: Springer.

Muller, E. B., & Nisbet, R. M. (2014). Dynamic energy budget modeling reveals the potential of future growth and calcification for the coccolithophore *E miliania huxleyi* in an acidified ocean. *Global change biology*, *20*(6), 2031-2038.

National Marine Fisheries Service (2018) Fisheries of the United States, 2017. U.S. Department of Commerce, NOAA Current Fishery Statistics No. 2017 Available at: https://www.fisheries.noaa.gov/feature-story/ fisheries-united-states-2017

Ní Longphuirt, S., Eschmann, C., Russell, C., & Stengel, D. B. (2013). Seasonal and species-specific response of five brown macroalgae to high atmospheric CO2. *Marine Ecology Progress Series*, 493, 91-102.

Papadakis, I. A., Kotzabasis, K., & Lika, K. (2005). A cell-based model for the photoacclimation and CO_2-acclimation of the photosynthetic apparatus. *Biochimica et Biophysica Acta (BBA)-Bioenergetics*, *1708*(2), 250-261.

Petrell, R. J., Tabrizi, K. M., Harrison, P. J., & Druehl, L. D. (1993). Mathematical model of *Laminaria* production near a British Columbian salmon sea cage farm. *Journal of Applied Phycology*, *5*(1), 1-14.

Poggiale, J. C., Baklouti, M., Queguiner, B., & Kooijman, S. A. L. M. (2010). How far details are important in ecosystem modelling: the case of multi-limiting nutrients in phytoplankton–zooplankton interactions. *Philosophical Transactions of the Royal Society of London B: Biological Sciences*, *365*(1557), 3495-3507.

Raven, J. A., Ball, L. A., Beardall, J., Giordano, M., & Maberly, S. C. (2005). Algae lacking carbon-concentrating mechanisms. *Canadian Journal of Botany*, *83*(7), 879-890.

R Core Team (2019). R: A language and environment for statistical computing. R Foundation for Statistical Computing, Vienna, Austria. URL https://www.R-project.org/.

Redmond, S., L.A. Green, C. Yarish, J. Kim, & C.D. Neefus. 2014. New England seaweed culture handbook: nursery systems. *Connecticut Sea Grant College Program.* CTSG-14-01. 92 pp. Available at: https://seagrant.uconn.edu/2014/01/01/new-england-seaweed-culture- handbook-nursery-systems/

Schaffelke, B., & Lüning, K. (1994). A circannual rhythm controls seasonal growth in the kelps *Laminaria hyperborea* and *L. digitata* from Helgoland (North Sea). *European Journal of Phycology*, *29*(1), 49-56.

Schiener, P., Black, K. D., Stanley, M. S., & Green, D. H. (2015). The seasonal variation in the chemical composition of the kelp species *Laminaria digitata*, *Laminaria hyperborea*, *Saccharina latissima* and *Alaria esculenta*. *Journal of Applied Phycology*, *27*(1), 363-373.

Segarra, K. E. A. 2002. Source Or Sink? Analysis of Narragansett Bay's carbon cycle. Brown University. Center for Environmental Studies.

Sjøtun, K. (1993). Seasonal lamina growth in two age groups of *Laminaria saccharina* (L.) Lamour. in western Norway. *Botanica marina*, *36*(5), 433-442.

Soetaert, K., & Petzoldt, T. (2010). Inverse modelling, sensitivity and Monte Carlo analysis in R using package FME. *Journal of Statistical Software*, *33*(3), 1-28.

Soetaert, K., Petzoldt, T. R., & Setzer, W. (2010). Solving Differential Equations in R: Package deSolve. Journal of Statistical Software, 33(9), 1-25. URL http://www.jstatsoft.org/v33/i09/ DOI 10.18637/jss.v033.i09

Taylor, W. R. (1972). *Marine algae of the eastern tropical and subtropical coasts of the Americas*. University of Michigan.

Ullman, D. S. & Codiga, D. L. (2010) *Characterizing the Physical Oceanography of Coastal Waters Off Rhode Island, Part 2: New Observations of Water Properties, Currents, and Waves.* Retrieved from https://www.seagrant.gso.uri.edu/oceansamp/pdf/appendix/03-PhysOcPart2-OSAMP-UllmanCodiga2010.pdf

Vettori, D., & Nikora, V. (2017). Morphological and mechanical properties of blades of *Saccharina latissima*. *Estuarine, Coastal and Shelf Science*, *196*, 1-9.

Willett, W., Rockström, J., Loken, B., Springmann, M., Lang, T., Vermeulen, S., ... & Jonell, M. (2019). Food in the Anthropocene: the EAT–Lancet Commission on healthy diets from sustainable food systems. *The Lancet*, *393*(10170), 447-492.

Wu, R. S. S. (1995). The environmental impact of marine fish culture: towards a sustainable future. *Marine Pollution Bulletin*, *31*(4-12), 159-166.

7. Tables

Table 1. Sugar kelp DEB model parameters and units resulting from fitting the model to the compiled literature and field data.

Parameter symbol	Parameter description	Parameter Units	Value	Source
$\dot{J}_{E_N Am}$	Maximum volume specific nitrogen assimilation	mol N mol M_V^{-1} h^{-1}	2.7 *10^{-4}	Espinoza and Chapman (1983)
K_N	Half-saturation concentration for NO_3^- and NH_4^+ uptake	mol NO_3^- and NH_4^+ L^{-1}	2.667 *10^{-6}	Espinoza and Chapman (1983)
$\dot{J}_{CO_2 m}$	Maximum volume specific CO_2 uptake rate	mol CO_2 mol M_V^{-1} h^{-1}	0.0075	This study
K_C	Half-saturation concentration for CO_2 uptake	mol CO_2 L^{-1}	4 *10^{-6}	This study
ρ_{PSU}	Photosynthetic unit (PSU) density	mol PSU mol M_V^{-1}	0.05	Johansson and Snoeijs (2002)
$\dot{b}_I$	Binding probability of a photon to a free light SU	_____	2.8 *10^{-6}	Johansson and Snoeijs (2002)
$\dot{k}_I$	Dissociation rate of releasing ATP and $NADPH^+$	mol NADPH mol PSU^{-1} h^{-1}	0.28	Johansson and Snoeijs (2002)
y_{IC}	Yield factor of C reserve to NADPH	mol NADPH mol EC^{-1}	2	Lavaud et al. (under review)
$y_{CO_2 C}$	Yield factor of C reserve to CO_2	mol CO_2 mol EC^{-1}	1	Lavaud et al. (under review)
$\dot{J}_{E_C Am}$	Maximum volume specific carbon assimilation	mol C mol M_V^{-1} h^{-1}	0.282	This study
$\dot{k}_{EC}$	Carbon reserve turnover rate	h^{-1}	0.05	This study
$\dot{k}_{EN}$	Nitrogen reserve turnover rate	h^{-1}	0.01	This study
$\dot{J}_{E_N M}$	Volume specific maintenance cost paid by N reserve	mol EN mol M_V^{-1} h^{-1}	3.2 *10^{-5}	This study

$\dot{J}_{E_C M}$	Volume specific maintenance cost paid by C reserve	mol EC mol M_V^{-1} h^{-1}	1.4 *10^{-5}	This study
$y_{E_N V}$	Yield factor of N reserve to structure	mol EN mol M_V^{-1}	0.04	Lorena et al. (2010)
$y_{E_C V}$	Yield factor of C reserve to structure	mol EC mol M_V^{-1}	1	This study
κ_{E_i}	Fraction of rejection flux incorporated back in i-reserve	_____	0.9	This study
T_A	Arrhenius temperature	K	6314.3	This study
T_0	Reference temperature	K	293.15	DEB theory standard
T_H	Upper boundary of temperature tolerance	K	286.536	This study
T_L	Lower boundary of temperature tolerance	K	273.15	This study
T_{AH}	Arrhenius temperature outside T_H	K	18702	This study
T_{AL}	Arrhenius temperature outside T_L	K	4391.9	This study
ω_V	Molar weight of structure	g mol^{-1}	29.89	C:H:O:N; 1: 1.33:1:0.04
ω_{EC}	Molar weight of C reserve	g C mol C^{-1}	30	C:H:O:N; 1:0.5:2.5:0
ω_{EN}	Molar weight of N reserve	g N mol N^{-1}	17	C:H:O:N; 0:1.5:1.5:1
ω_{O_2}	Molar weight of O_2	g O_2 mol O_2^{-1}	32	Periodic Table

Table 2. Model equations with environmental conditions: T = temperature (K), I = irradiance (µE m^{-2} h^{-1}), DIC = dissolved inorganic carbon (mol DIC L^{-1}), and N = nitrate and ammonium concentration (NO_3^- and NH_4^+ L^{-1}).

Equation	Equation description
$C_T = exp\left(\frac{T_A}{T_0} - \frac{T_A}{T}\right)\left[1 + exp\left(\frac{T_{AL}}{T_0} - \frac{T_{AL}}{T_L}\right) + exp\left(\frac{T_{AH}}{T_H} - \frac{T_{AH}}{T_0}\right)\right]\left[1 + exp\left(\frac{T_{AL}}{T} - \frac{T_{AL}}{T_L}\right) + exp\left(\frac{T_{AH}}{T_H} - \frac{T_{AH}}{T}\right)\right]^{-1}$	temperature correction
$\dot{J}_{E_N A} = \dot{J}_{E_N Am} * C_T * [\mathbf{N}]/([\mathbf{N}] + K_N)$	specific assimilation rate of N
$\dot{J}_{CO_2} = (\dot{J}_{CO_2 m} * C_T) * ([\mathbf{DIC}]/[\mathbf{DIC}] + K_C))$	specific CO_2 uptake rate

$$\dot{J}_I = \frac{\rho_{PSU} * I * \dot{b}_I}{1 + \frac{I * \dot{b}_I}{\dot{k}_I * C_T}}$$	specific relaxation rate
$$\dot{J}_{O_2} = \frac{\dot{J}_I * M_V * \omega_{O_2}}{B * 4}$$	oxygen production rate
$$\dot{J}_{E_C A} = (\frac{1}{\dot{J}_{E_C Am} * C_T} + \frac{1}{\dot{J}_{CO_2}/y_{CO_2 C}} + \frac{1}{\dot{J}_I/y_{IC}} - \frac{1}{\dot{J}_I/y_{IC} + \dot{J}_{CO_2}/y_{CO_2 C}})^{-1}$$	specific assimilation rate of C
$$\dot{J}_{E_i C} = m_{E_i}(\dot{k}_{E\iota} * C_T) - \dot{r})$$	specific catabolic flux of N or C reserve
$$\dot{r} = \frac{1}{M_V}\frac{dM_V}{dt}$$	net specific growth rate
$$\dot{J}_{E_i}^{M_i} = \min(\dot{J}_{E_i C}, (\dot{J}_{E_i M} * C_T))$$	specific flux for metabolism from N or C reserve
$$\dot{J}_{E_i G} = \dot{J}_{E_i C} - \dot{J}_{E_i}^{M_i}$$	specific growth flux from N or C reserve
If $\dot{J}_{E_i}^{M_i} < \dot{J}_{E_i M} * C_T$ $$\dot{J}_V^M = \sum_i \dot{J}_{V_i}^{M_i} = \sum_i \left[\left((\dot{J}_{E_i M} * C_T) - \dot{J}_{E_i}^{M_i}\right) y_{E_i V}^{-1}\right]$$	specific maintenance flux from structure
$$\dot{J}_{VG} = \dot{r} + \dot{J}_V^M = \left[\sum_i \left(\frac{\dot{J}_{E_i G}}{y_{E_i V}}\right)^{-1} - \left(\sum_i \frac{\dot{J}_{E_i G}}{y_{E_i V}}\right)^{-1}\right]^{-1}$$	specific gross growth rate
$$\dot{J}_{E_i R} = \dot{J}_{E_i G} - y_{E_i V} * \dot{J}_{VG}$$	rejected specific C or N flux from growth SU
$$\frac{d}{dt} m_{E_i} = \dot{J}_{E_i A} - \dot{J}_{E_i C} + \kappa_{E_i} * \dot{J}_{E_i R} - \dot{r} * m_{E_i}$$	dynamics of the N or C reserve
$$\frac{d}{dt} M_V = \dot{r} * M_V$$	dynamics of structural mass
$$B = (\omega_V + m_{E_C} * \omega_{EC} + m_{E_N} * \omega_{EN}) * M_V$$	modeled kelp blade biomass
$$L = (\frac{B}{0.00387})^{(\frac{1}{1.469})}$$	length in cm from an allometric relationship between length and dry weight from Gevaert et al. (2001)

Table 3. Data from literature and this study used to calibrate our sugar kelp DEB model.

Reference	**Location**	Data	Experimental conditions	Time period
Espinoza and Chapman (1983)	Nova Scotia, Canada	NO^{3-} uptake (µg N g_{DW}^{-1} h^{-1})	T° = 9 and 18 °C [N] = from 2.5 to 88 µM NO^{3-}	Discrete measurements
Johansson and Snoeijs (2002)	Sweden	Photosynthesis Rate	T° = 14 °C I = 0-900 µE m^{-2} s^{-1}	Discrete measurements
*Davison (1987)	Germany	Photosynthesis rates (µmol C g f. wt^{-1} h^{-1})	T° = 0 to 30 °C with 5 °C intervals I = 200 µE m^{-2} s^{-1}	Discrete measurements
*Fortes and Lüning (1980)	Germany	Specific growth rate (% day^{-1})	T° = 0, 5, 10, 15, and 20 °C I = 70 µE m^{-2} s^{-1}	7 days
*Bolton and Lüning (1982)	Germany, UK, France, and Norway	Specific growth rate (% day^{-1})	T° = 0, 5, 10, 15, 20, and 23 °C I = 50 µE m^{-2} s^{-1}	7 days
*Davison and Davison (1987)	Germany	Relative growth rate (cm cm^{-1} $month^{-1}$)	T° = 0, 5, 10, 15 and 20 °C I = 60 µE m^{-2} s^{-1}	1 month
This study	Rhode Island, USA	Blade length (cm) and N:C ratio (mol mol^{-1})	T° = 1.5-20 °C [N] = $7.65e^{-7}$-$1.2e^{-5}$ M NO_3^- and NH_3 [C] = $1.836e^{-3}$ mol DIC/L at Pt. Judith Pond sites (J. Grear, unpublished data) and $1.956e^{-3}$ mol DIC/L for Narragansett Bay sites (Segarra, 2002) I = 0-$2e^{+6}$ daily µE m^{-2} h^{-1}	2 seasons (2017-2018, and 2018-2019) with kelp growth ranging from 138 to 172 days on the farm

*Used only to build the Arrhenius relationship

Table 4. End of season length growth of kelp blades in cm (±SD) at each site.

Season	Nar. Bay N	Nar. Bay S, L1	Nar. Bay S, L2	Pt Judith Pond N, L1	Pt Judith Pond N, L2	Pt Judith Pond S, L1	Pt Judith Pond S, L2
2017-2018	67.9 (± 22.6)	133.4 (± 78.8)	73.2 (± 17.6)	74.8 (± 18.3)	81.0 (± 34.8)	85.9 (± 37.1)	87.3 (± 32.0)
2018-2017	50.5 (± 13.0)	65.3 (± 22.5)	20.0 (± 6.8)	80.1 (± 23.1)	46.9 (± 14.7)	63.8 (± 26.3)	47.1 (± 10.9)

8. Figures

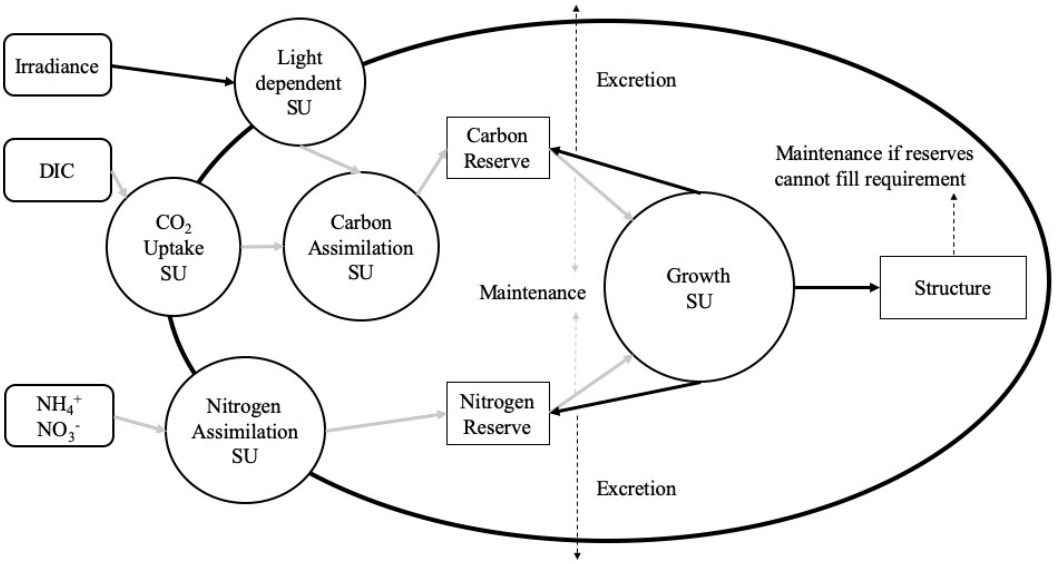

Figure 1. Sugar kelp DEB model concept map based on Lorena et al. (2010) and Lavaud et al. (under review). The large oval represents the algae and the surrounding area is its environment. Rectangles with curved corners are the modeled inputs to the kelp. Rectangles with square corners are the state variables of the model, representing the main pools of mass in the modeled organism. Circles are synthesizing units. Dotted arrows represent fluxes of mass leaving the main model system either through excretion or use in maintenance. Grey arrows depict where the temperature correction is applied to a parameter of the model.

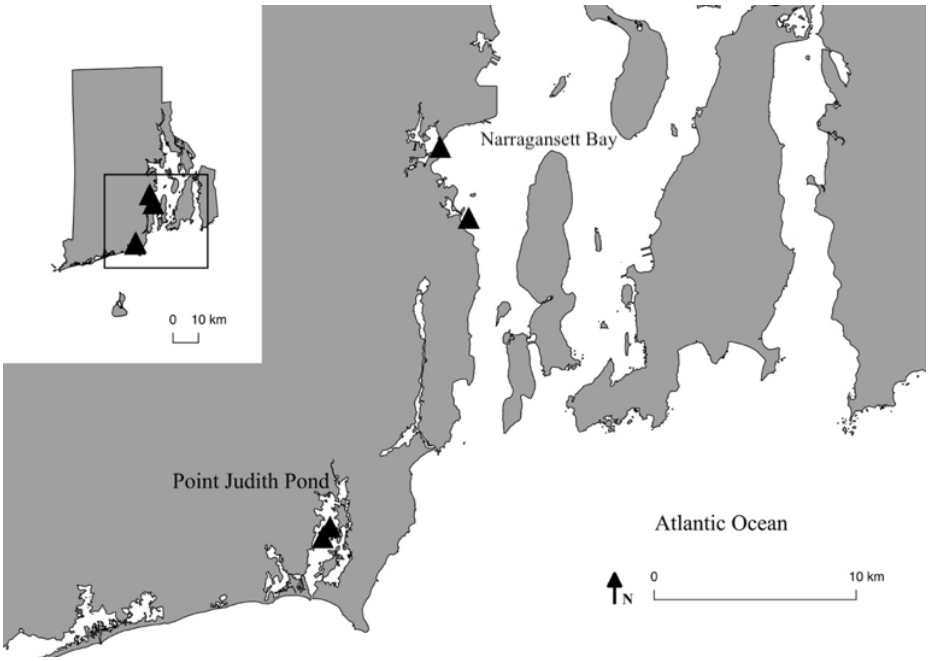

Figure 2. Sugar kelp was grown on RI oyster farms at the black triangles for this study.

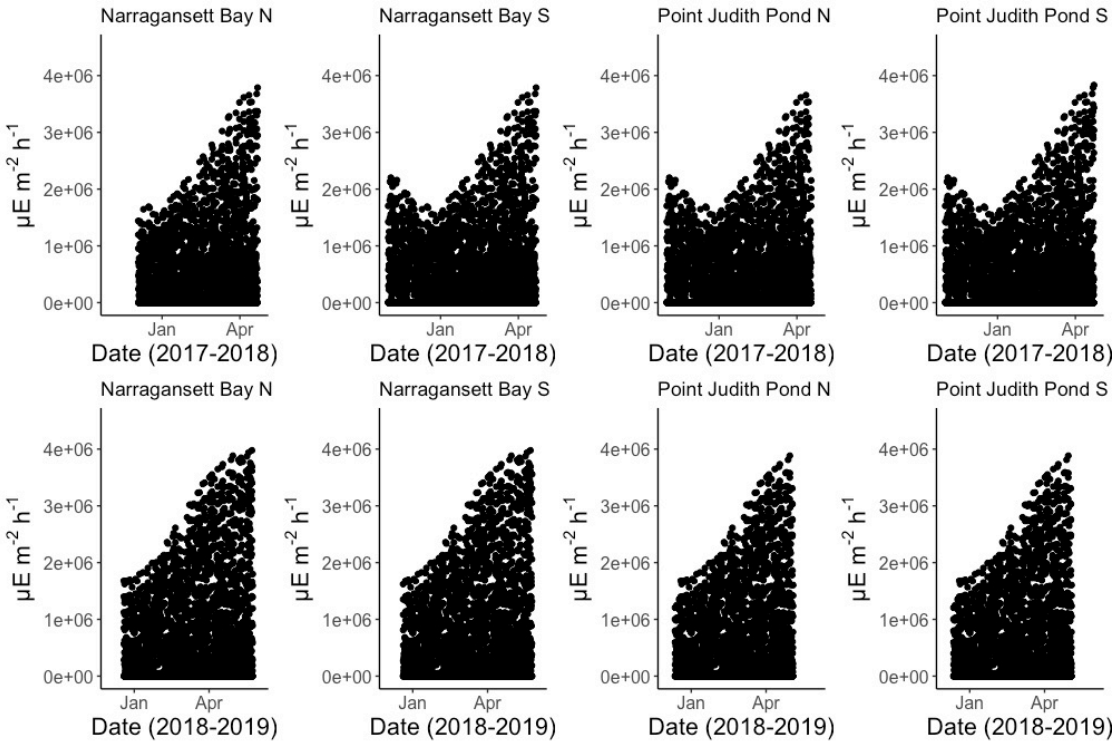

Figure 3. Irradiance forcing used for the 2017-2018 kelp season (top row) and the 2018-2019 kelp season (bottom row) from converted from the radiative forcing from the North American Regional Reanalysis.

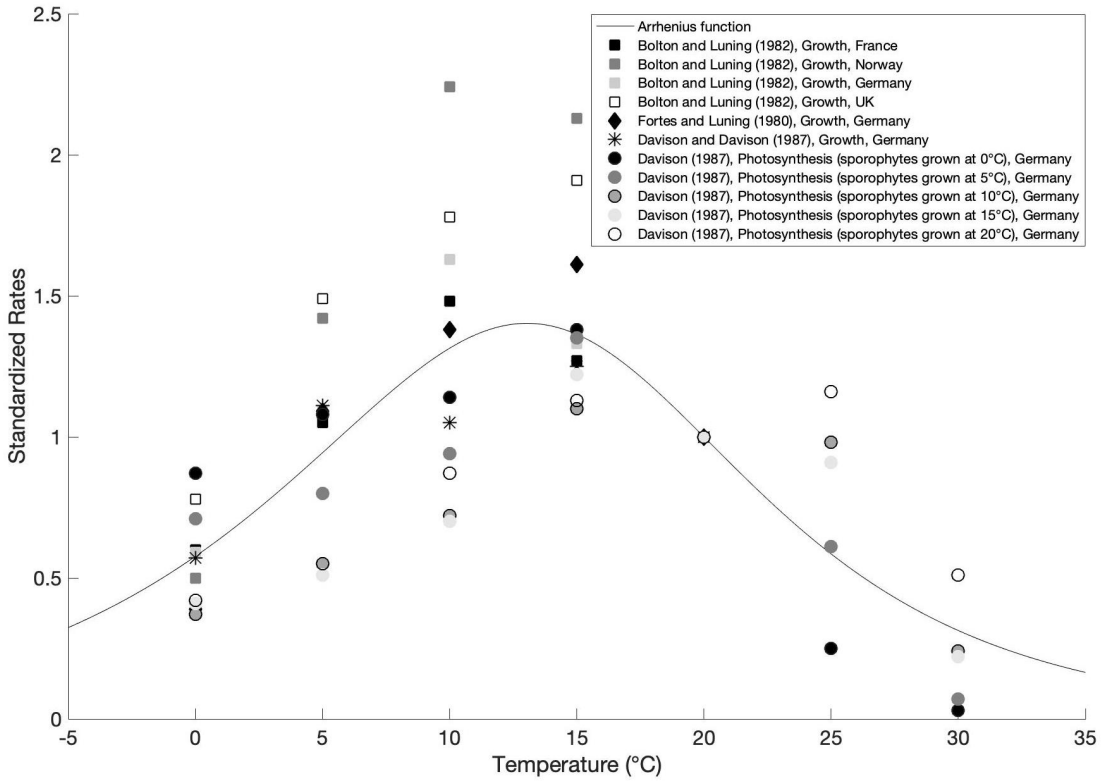

Figure 4. The Arrhenius relationship for *S. latissima* was estimated using multiple growth and photosynthesis datasets: 1) Bolton and Lüning (1982) (squares; black for kelp from France, dark grey for Norway, light grey for Germany, white for the UK), 2) Fortes and Lüning (1980) (diamond), 3) Davison and Davison (1987) (asterisk), and 4) Davison (1987) (circles; black for sporophyte rearing temp 0°C, dark grey for 5°C, dark grey with black border for 10°C, light grey for 15°C, and white for 20°C). The adjusted R-squared statistic for the fit of the curve to the data points is 0.551 (p-value = 2.74e-11).

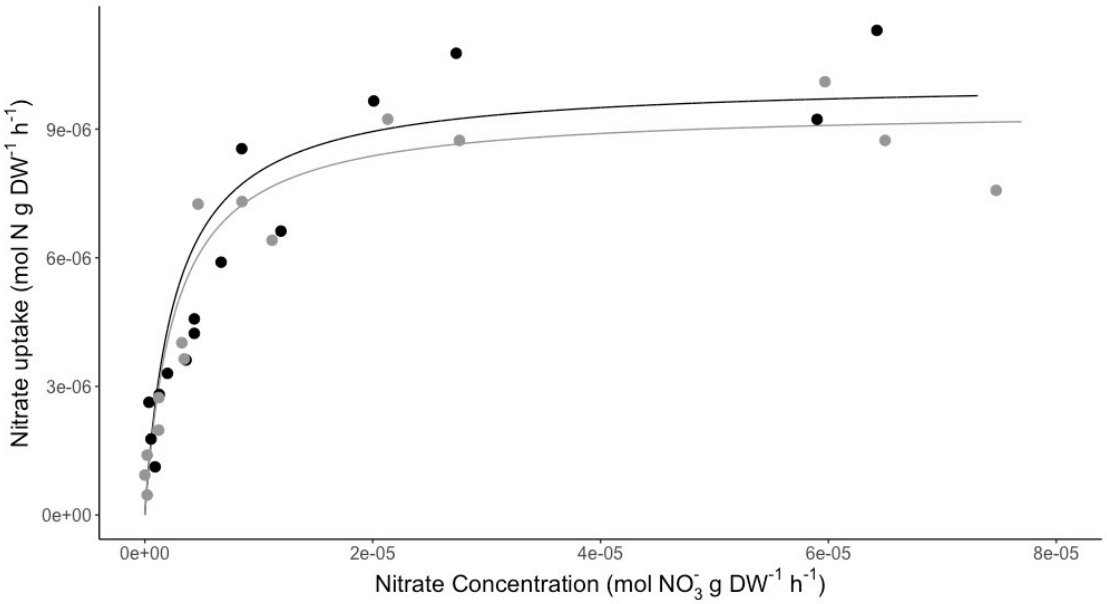

Figure 5. Modeled (lines) and observed (dots) nitrate (and ammonium, only in model) uptake from Espinoza and Chapman (1983). Black depicts the uptake at 9°C and grey illustrates the uptake at 18°C. The RMSE for the model calibrated to the 9°C data is 1.43e-06 and 9.73e-07 (both mol N gDW^{-1} h^{-1}) for the model calibrated to the data collected at 18°C.

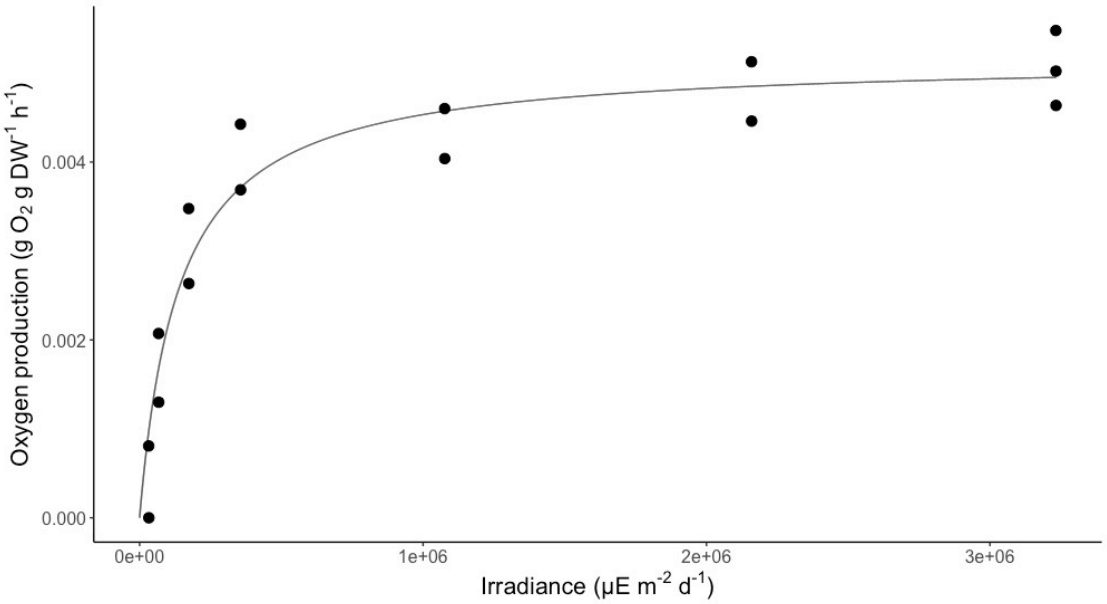

Figure 6. Modeled (lines) and observed (dots) oxygen production from Johansson and Snoeijs (2002). The RMSE for the fit of this model curve to this data is 0.000457 (g O_2 g DW^{-1} h^{-1}).

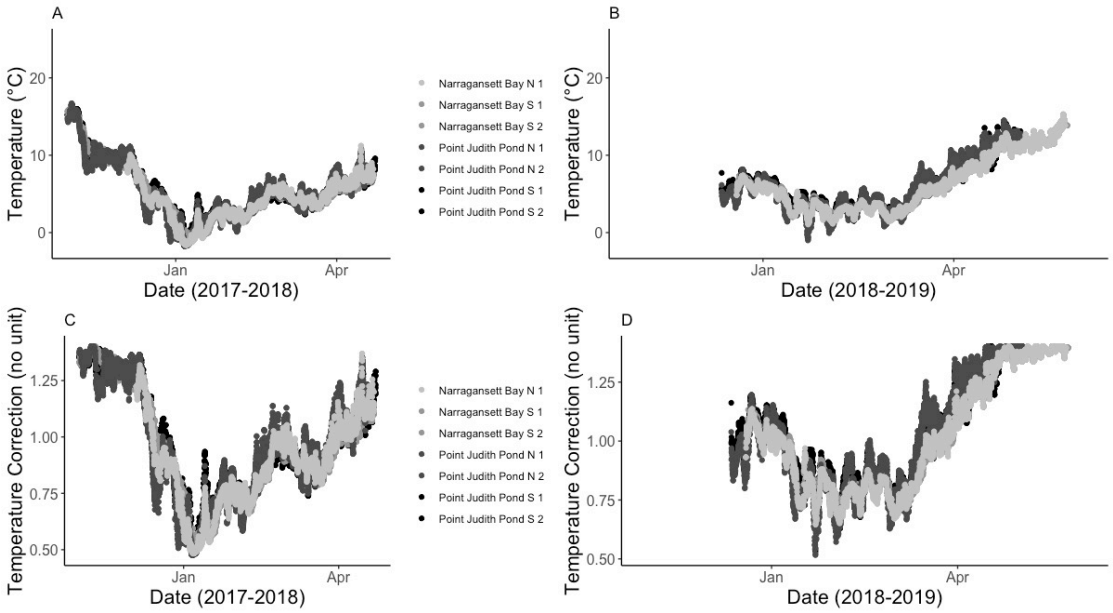

Figure 7. Temperature (°C) field data from the 2017-2018 kelp season (A) and the 2018-2019 kelp season (B). Temperature correction factor calculated using the Arrhenius equation and temperature field data from the 2017-2018 kelp season (C) and the 2018-2019 kelp season (D).

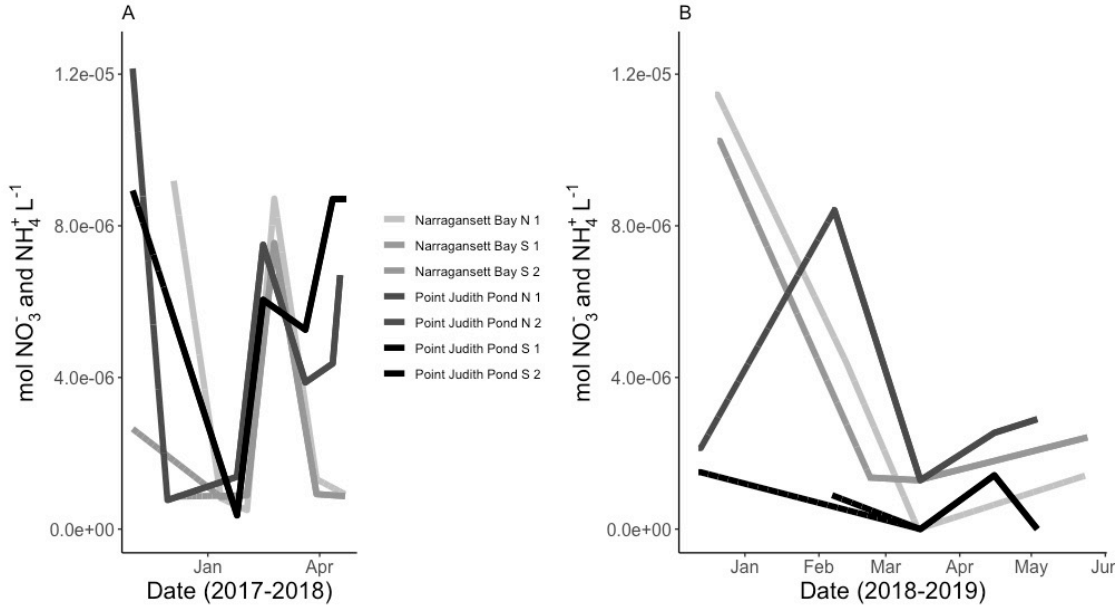

Figure 8. Nitrate and ammonium concentration forcing data used for the 2017-2018 kelp season (A) and the 2018-2019 kelp season (B) from field data points.

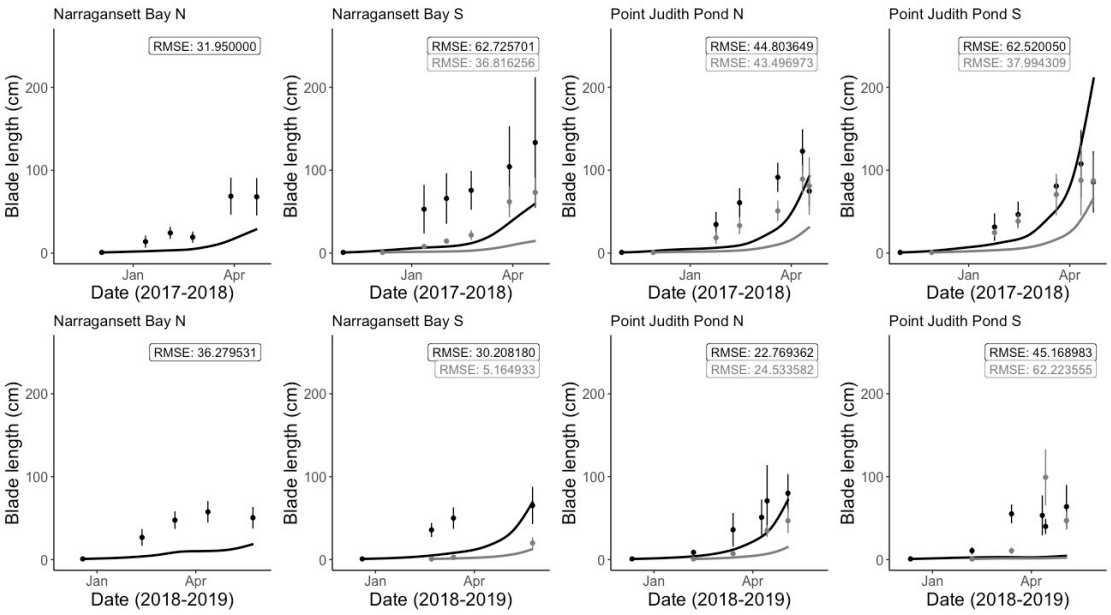

Figure 9. *Saccharina latissima* blade length growth (cm) from the 2017-2018 growing season (top row) and the 2018-2019 growing season (bottom row). Dots with error bars depict the mean length from the field data and the standard deviation. The lines are the prediction of the *S. latissima* DEB model. Lines and dots in black are the first kelp line planted at a site, and those in grey depict the second kelp line planted later in the year.

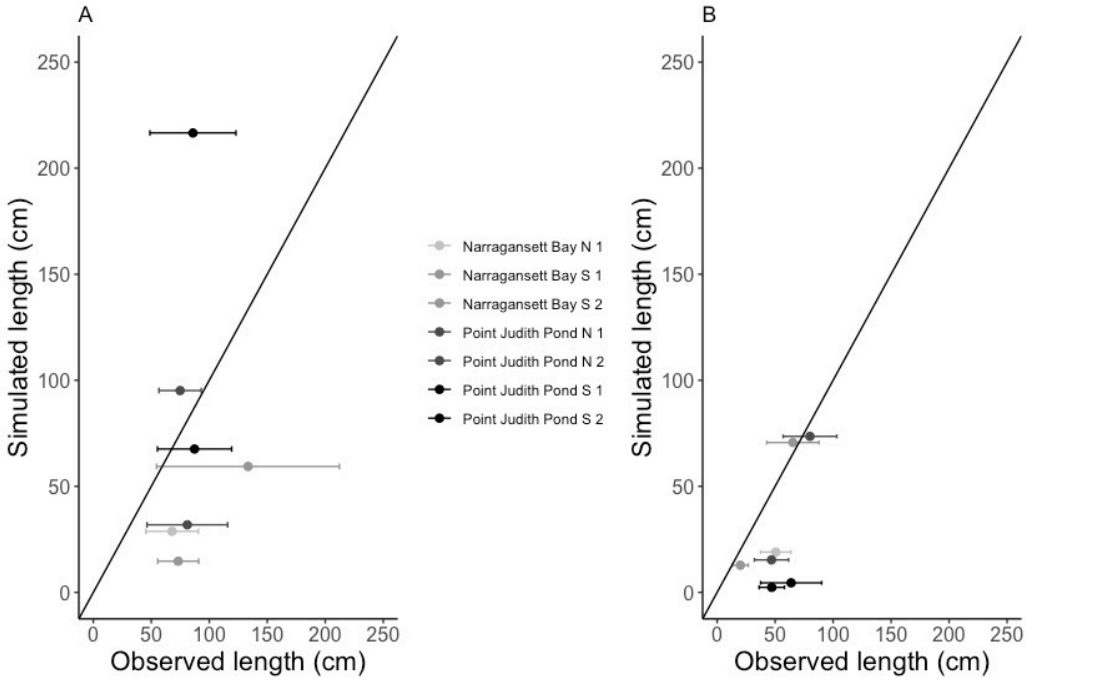

Figure 10. Regression plot of observed versus simulated *S. latissima* length (cm) for all sites in (A) 2017-2018 season and (B) 2018-2019 season. Error bars show standard deviation. The black diagonal line shows the one to one relationship between observed and simulated length.

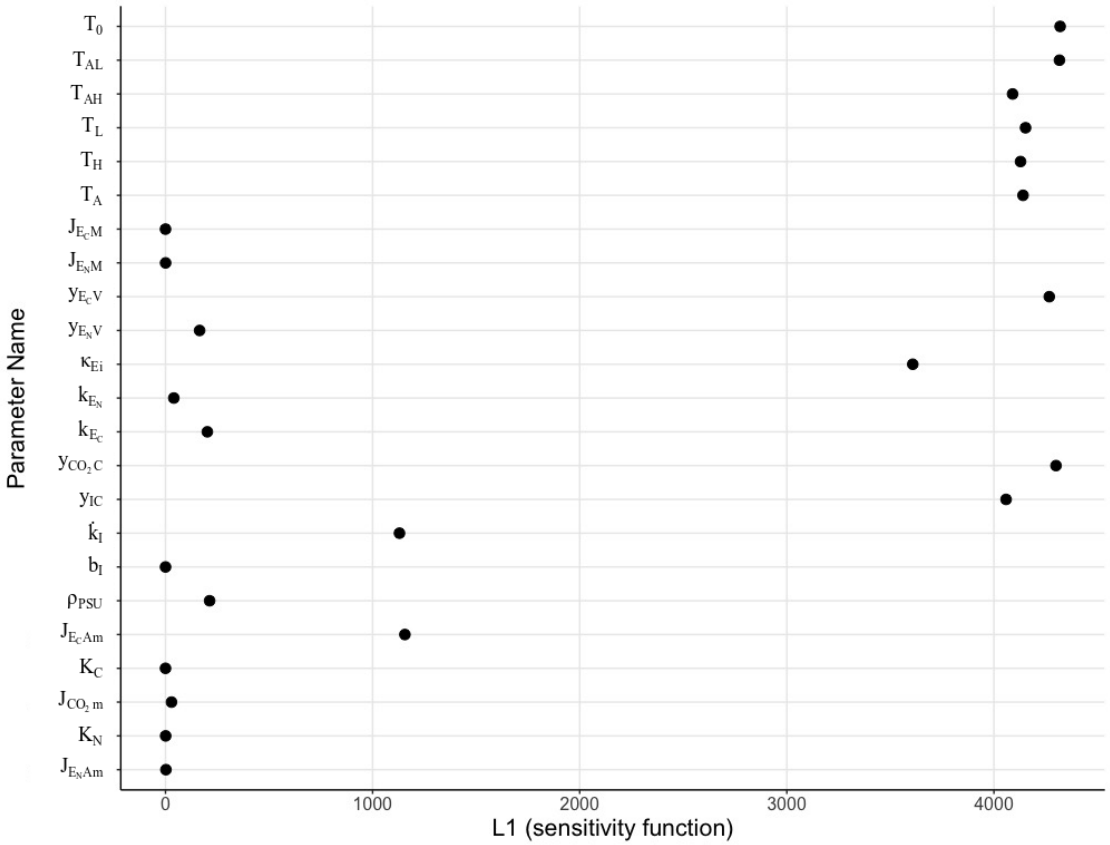

Figure 11. Sensitivity of $\boldsymbol{m_{E_C}}$, $\boldsymbol{m_{E_N}}$, and $\boldsymbol{M_V}$ to model parameters using the L1 sensitivity function.

SUPPORTING INFORMATION

Appendix S1: Model Initial Conditions and Molecular Weights

Table S1a. Initial conditions used in all model runs for the Rhode Island field data.

Carbon reserve density (m_{E_C}) (mol EC / mol M_V)	Nitrogen reserve density (m_{E_N}) (mol EN / mol M_V)	Mass of structure (M_V) (g)	Blade biomass dry weight (B) (g)	Blade Length (L) (cm)
0.1	0.03	0.00009	0.003006	0.8419928

Table S1b. Molecular weights.

Molecular weight of structure (ω_V) (g/mol)	Molecular weight of nitrogen reserve (ω_{EN}) (g/mol)	Molecular weight of carbon reserve (ω_{EC}) (g/mol)
29.89	17	30

Initial reserve densities were set based on the knowledge that the carbon reserve would occupy a larger amount of mass in comparison to the nitrogen reserve at the starting time of the study. Initial blade lengths and biomass were set together using the Gevaert et al. (2001) power relationship to set a length similar to that of the sporophytes on the day they were planted out on the farms. Initial mass of structure was set to calculate the chosen initial blade biomass. The molecular weights used in this biomass calculation were calculated from assumed C:H:O:N chemical compositions and the associated atomic masses of these elements. The nitrogen reserve's chemical composition is ammonia, the carbon reserve's chemical composition is glucose, laminarin, and mannitol, and the structure's chemical composition is the average of mannitol and laminarin. Because structure is also composed of a significant amount of proteins, we set the structure chemical index for N to 0.04.

Appendix S2: Model Equation Descriptions

A temperature correction (C_T) is applied to all modelled rates expect for the photon binding rate ($\dot{b}_I$) (Lorena et al., 2010, Lavaud et al., under review). Arrhenius relationships are based on the idea that metabolic rates of a species are impacted the same amount by temperature change (Kooijman, 2010). This correction is an extended Arrhenius correction factor; the extension supports a non-linear response to temperature change:

$$C_T = exp\left(\frac{T_A}{T_0} - \frac{T_A}{T}\right)\left[1 + exp\left(\frac{T_{AL}}{T_0} - \frac{T_{AL}}{T_L}\right) + exp\left(\frac{T_{AH}}{T_H} - \frac{T_{AH}}{T_0}\right)\right]\left[1 + exp\left(\frac{T_{AL}}{T} - \frac{T_{AL}}{T_L}\right) + exp\left(\frac{T_{AH}}{T_H} - \frac{T_{AH}}{T}\right)\right]^{-1}$$

With T_A the Arrhenius temperature, T_0 the reference temperature, T is the field or input temperature, T_L and T_H the lower and higher bounds of temperature tolerance, and T_{AL} and T_{AH} the Arrhenius temperatures for the lower and higher temperatures outside the optimal range (all in K).

In this model, rates (variables with dotted letters) are expressed per C-mol of structure. The specific assimilation rate of nitrate and ammonium ($\dot{J}_{E_NA}$ in mol N mol M_V^{-1} h^{-1}) is calculated through a Michaelis-Menten relationship:

$$\dot{J}_{E_NA} = \dot{J}_{E_NAm} * C_T * [N]/([N] + K_N)$$

With $\dot{J}_{E_NAm}$ maximum volume specific nitrogen assimilation (mol N mol M_V^{-1} h^{-1}), [N] the concentration of ammonium and nitrate in the environment (NO_3^- and NH_4^+ L^{-1}), and K_N half-saturation concentration for NO_3^- and NH_4^+ uptake (mol NO_3^- and NH_4^+ L^{-1}).

Both carbon and nitrogen assimilation are described as synthesizing units (SUs) in DEB theory. SUs are a simple way to depict conversions of mass from one state to another within an organism. They function under rules similar to classic

enzyme kinetics with a major difference being the assumption of low substrate-enzyme dissociation rates (Kooijman, 2010). SUs allow for dynamic substrate limitation and flexible computation. For carbon dynamics in particular three linked SUs model the different parts of photosynthesis. One of these SUs facilitates the uptake of carbon dioxide. The specific CO_2 uptake rate ($\dot{J}_{CO_2}$ in mol CO_2 mol M_V^{-1} h^{-1}) is calculated through a Michaelis-Menten relationship similarly to $\dot{J}_{E_NA}$ in this model:

$$\dot{\boldsymbol{J}}_{\boldsymbol{CO_2}} = (\dot{\boldsymbol{J}}_{\boldsymbol{CO_2 m}} * \boldsymbol{C_T}) * ([\boldsymbol{DIC}]/ [\boldsymbol{DIC}] + \boldsymbol{K_C})$$

With $\dot{J}_{CO_2 m}$ maximum volume specific CO_2 uptake rate (mol CO_2 mol M_V^{-1} h^{-1}), [DIC] the concentration of dissolved inorganic carbon (mol DIC L^{-1}), and K_C half-saturation concentration for CO_2 uptake (mol DIC L^{-1}). Bicarbonate is converted to carbon dioxide by carbonic anhydrase, so this is why the forcing is DIC and what is being taken in is CO_2.

Another of the photosynthesis SUs depicts the light-dependent reactions of photosynthesis. In this equation, photons are bound to photosystems and ATP and NADPH are produced and released at set rates. The specific relaxation rate ($\dot{J}_I$ in mol NADPH mol M_V^{-1} h^{-1}) is given by:

$$\dot{\boldsymbol{J}}_{\boldsymbol{I}} = \frac{\boldsymbol{\rho_{PSU}} * \boldsymbol{I} * \dot{\boldsymbol{b}}_{\boldsymbol{I}}}{\mathbf{1} + \frac{\boldsymbol{I} * \dot{\boldsymbol{b}}_{\boldsymbol{I}}}{\dot{\boldsymbol{k}}_{\boldsymbol{I}} * \boldsymbol{C_T}}}$$

With ρ_{PSU} photosynthetic unit (PSU) density (mol PSU mol M_V^{-1}), I forcing function irradiance (µE m^{-2} h^{-1}), $\dot{b}_I$ photon binding rate (unitless), and $\dot{k}_I$ dissociation rate of releasing ATP and $NADPH^+$ (mol NADPH mol PSU^{-1} h^{-1}).

The final SU of the carbon dynamics integrates the inputs of the previous two SUs and assimilates carbon to its reserve. This part of the photosynthesis model

represents the Calvin-Benson cycle during which carbohydrates are formed from carbon dioxide. The specific assimilation rate of C ($\dot{J}_{E_CA}$ in mol C mol M_V^{-1} h^{-1}) is calculated through the parallel processing of NADPH and CO_2:

$$\dot{J}_{E_CA} = \left(\frac{1}{\dot{J}_{E_CAm} * C_T} + \frac{1}{\dot{J}_{CO_2}/y_{CO_2C}} + \frac{1}{\dot{J}_I/y_{IC}} - \frac{1}{\dot{J}_I/y_{IC} + \dot{J}_{CO_2}/y_{CO_2C}}\right)^{-1}$$

With $\dot{J}_{E_CAm}$ maximum volume specific carbon assimilation (mol C mol M_V^{-1} h^{-1}), y_{CO_2C} yield factor of C reserve to CO_2 (mol CO_2 mol EC^{-1}), and y_{IC} yield factor of C reserve to NADPH (mol NADPH mol EC^{-1}).

Oxygen is produced as a byproduct of the reduction of NADP+, and one mole of O_2 is produced for every four moles of NADPH produced. Calculating the oxygen production rate ($\dot{J}_{O_2}$ in g O_2 g biomass^{-1} h^{-1}) is a useful equation in this model to provide comparisons to literature data to calibrate the photosynthesis parameters:

$$\dot{J}_{O_2} = \frac{\dot{J}_I * M_V * \omega_{O_2}}{B * 4}$$

With M_V structural mass (mol M_V), ω_{O_2} molar weight of O_2 (g O_2 mol O_2^{-1}), and B is modeled kelp blade biomass (g).

Reserves are catabolized to send mass on to be used in growth or maintenance. The specific catabolic flux of the N or C reserves (j_{E_iC} in mol EN or EC molM_V^{-1} h^{-1}) follows first order kinetics, which means that as the carbon or nitrogen reserve density (m_{E_i} in mol EN or EC mol M_V^{-1}) increases the faster catabolism will occur:

$$j_{E_iC} = m_{E_i}\left(\dot{k_{E_i}} * C_T\right) - \dot{r}\right)$$

With $\dot{k_{Ei}}$ carbon or nitrogen reserve turnover rate (h^{-1}) and $\dot{r}$ net specific growth rate (h^{-1}):

$$\dot{r} = \frac{1}{M_V}\frac{dM_V}{dt}$$

$\dot{r}$ is modified at each timestep using a function modified from the DEBtool package's function called *sgr2.m* in the alga section (https://www.bio.vu.nl/thb/deb/deblab/debtool/DEBtool_M/manual/index.html). The method that underlies this function is the Newton-Raphson method with continuation.

Maintenance takes priority over growth for catabolized resources in DEB theory. The specific flux for metabolism from the N or C reserves ($j_{E_i}^{M_i}$ in mol EN or EC mol Mv^{-1} h^{-1}) is set by the temperature corrected volume-specific maintenance cost paid by N or C reserve (j_{E_iM} in mol EN or EC mol Mv^{-1} h^{-1}) if the catabolic flux is enough to meet those costs:

$$j_{E_i}^{M_i} = \min\left(j_{E_iC}, (j_{E_iM} * C_T)\right)$$

The specific growth fluxes from both N and C reserves (j_{E_iG} in mol EN or EC mol Mv^{-1} h^{-1}) sent to the growth SU contain any mass left after maintenance costs are filled:

$$j_{E_iG} = j_{E_iC} - j_{E_i}^{M_i}$$

If maintenance requirements not met by the catabolic fluxes from the reserves, maintenance costs will be met by drawing from structure. The specific maintenance flux from structure (j_V^M in mol N and C mol Mv^{-1} h^{-1}) is given by:

$$j_V^M = \sum_i j_{V_i}^{M_i} = \sum_i \left[\left((j_{E_iM} * C_T) - j_{E_i}^{M_i}\right) y_{E_iV}{}^{-1}\right]$$

With y_{E_iV} yield factor of N reserve or C reserve to structure (mol EN or EC mol Mv^{-1}).

The growth SU handles growth fluxes from both reserves complementarily, so the specific gross growth rate (j_{VG} in h^{-1}) is given by:

$$\boldsymbol{j_{VG} = \dot{r} + j_V^M = \left[\sum_i \left(\frac{j_{E_iG}}{y_{E_iV}}\right)^{-1} - \left(\sum_i \frac{j_{E_iG}}{y_{E_iV}}\right)^{-1}\right]^{-1}}$$

Either the amount of carbon or nitrogen available will limit the growth SU, so excess will be available for one of the compounds. The model can reject this excess material as binding sites are filled and return it to the respective reserve. This rejected specific C or N flux from growth SU (j_{E_iR} in mol Ei mol M_V^{-1} h^{-1}) is the difference between available growth flux and what is actually used for growth:

$$\boldsymbol{j_{E_iR} = j_{E_iG} - y_{E_iV} * j_{VG}}$$

The dynamics of the state variables are the main differential equations of the model. The dynamics of the N or C reserve densities balance the inputs of assimilation and returning rejected flux with the outputs of catabolism and dilution by growth:

$$\boldsymbol{\frac{d}{dt} m_{E_i} = j_{E_iA} - j_{E_iC} + \kappa_{E_i} * j_{E_iR} - \dot{r} * m_{E_i}}$$

With κ_{E_i} fraction of rejection flux incorporated in i-reserve (unitless).

The dynamics of structural mass are controlled by the net specific growth rate:

$$\boldsymbol{\frac{d}{dt} M_V = \dot{r} * M_V}$$

Modeled kelp blade biomass (dry weight) is calculated by summing the mass of the reserves and the structure in the model:

$$\boldsymbol{B = (\omega_V + m_{E_C} * \omega_{EC} + m_{E_N} * \omega_{EN}) * M_V}$$

With $\boldsymbol{\omega_V}$ molar weight of structure (g mol^{-1}), $\boldsymbol{\omega_{EC}}$ molar weight of C reserve (g C mol C^{-1}), and $\boldsymbol{\omega_{EN}}$ molar weight of N reserve (g N mol N^{-1}).

Kelp blade length (cm) is calculated using an allometric relationship between length and dry weight from Gevaert et al. (2001):

$$L = \frac{B}{0.00387}^{\frac{1}{1.469}}$$

Appendix S3: Field Season Information

Table S3. Dates of kelp planting out on each farm site and harvest for both of the field seasons.

Season	Nar. Bay N	Nar. Bay S, L1	Nar. Bay S, L2	Pt Judith Pond N, L1	Pt Judith Pond N, L2	Pt Judith Pond S, L1	Pt Judith Pond S, L2
2017-2018: Plant Date	12/4/17	11/1/17	12/6/17	11/1/17	11/29/17	11/1/17	11/29/17
2017-2018: Harvest Date	4/21/18	4/21/18	4/21/18	4/17/18	4/17/18	4/22/18	4/22/18
2018-2019: Plant Date	12/19/18	12/20/18	2/21/19	12/12/18	2/6/19	12/12/18	2/6/19
2018-2019: Harvest Date	5/23/19	5/24/19	5/24/19	5/3/19	5/3/19	5/3/19	5/3/19

Appendix S4: Calculating Photosynthetically Active Radiation from Net Shortwave Radiation

To calculate PAR photosynthetically active radiation (μmol photons/m^2/h) from data from the North American Regional Reanalysis (Mesinger et al., 2006), we used this equation:

$$\mathbf{PAR = NSW*PAR\_frac*C*exp(-k*z)*3600}$$

With NSW net shortwave radiation (W/m^2) at the water surface calculated from downward shortwave flux minus upward shortwave flux, PAR_farc fraction of the incident flux useable for photosynthesis (unitless), C a conversion factor (μmol photons/s/W), k extinction coefficient (m^{-1}), z depth (m), and 3600 to convert from per second to per hour. C is a standard 4.56 (μmol photons/s/W) (Mõttus et al., 2011). We used a PAR_frac of 0.43 (Mõttus et al., 2011). We used 0.46 m^{-1} for k from past work in Narragansett Bay (Ullman & Codiga, 2010).

Appendix S5: Plots Related to Internal Model Dynamics

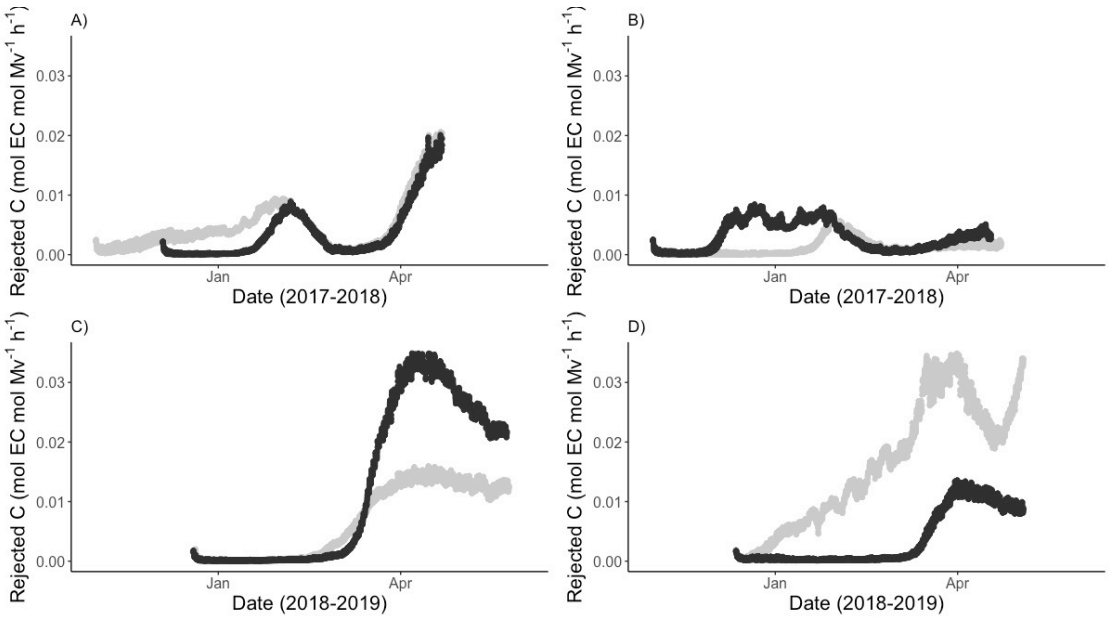

Figure S5a. Modeled carbon rejected flux from the carbon reserve for kelp lines from the 2017-2018 growing season (top row) and the 2018-2019 growing season (bottom row). Darker grey is for the north lines and the lighter grey is for the south lines. A) and C) are Narragansett Bay N and S and B) and D) are Pt. Judith Pond N and S.

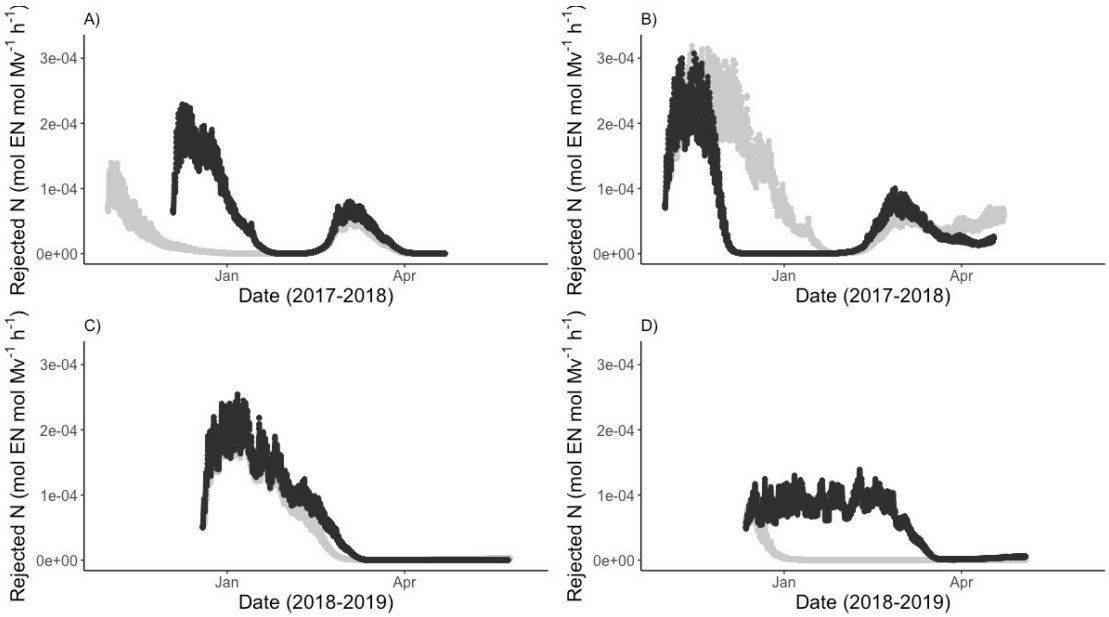

Figure S5b. Modeled rejected specific N flux from the growth synthesizing unit for kelp lines from the 2017-2018 growing season (top row) and the 2018-2019 growing season (bottom row). Darker grey is for the north lines and the lighter grey is for the south lines. A) and C) are Narragansett Bay N and S and B) and D) are Pt. Judith Pond N and S.

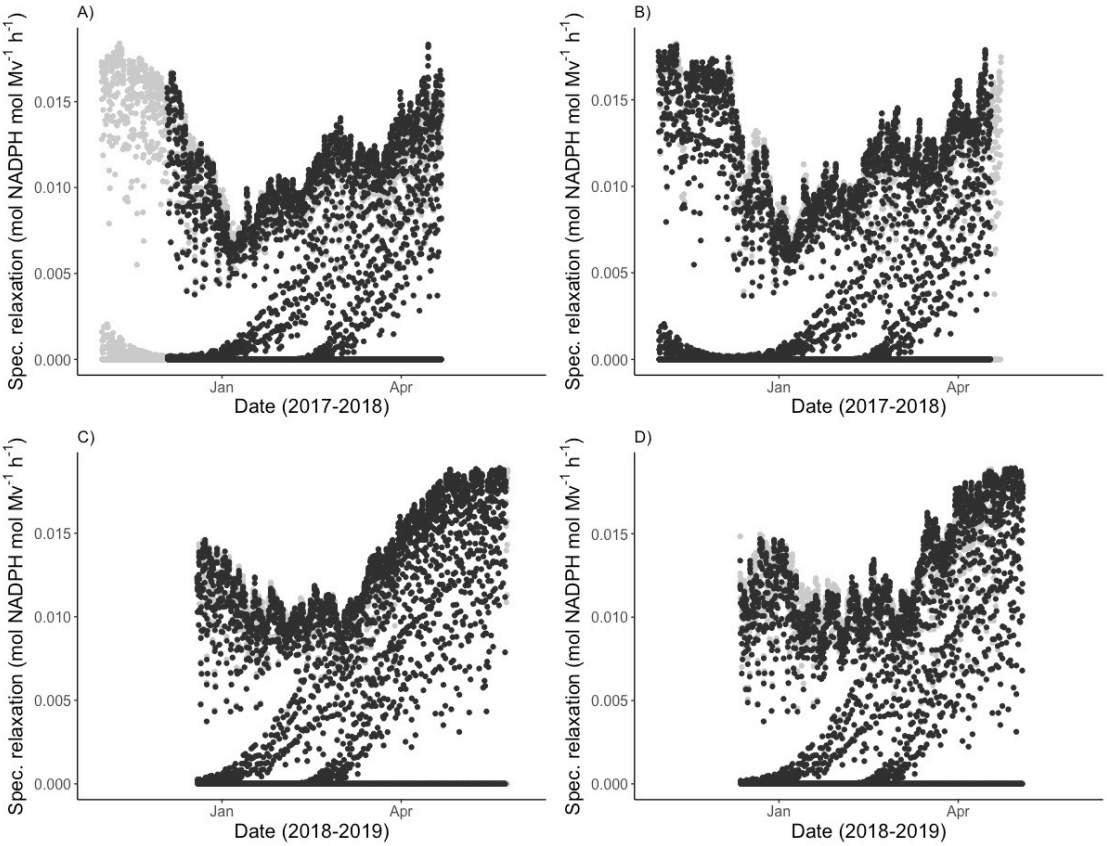

Figure S5c. Modeled specific relaxation rates for kelp lines from the 2017-2018 growing season (top row) and the 2018-2019 growing season (bottom row). Darker grey is for the north lines and the lighter grey is for the south lines. A) and C) are Narragansett Bay N and S and B) and D) are Pt. Judith Pond N and S.

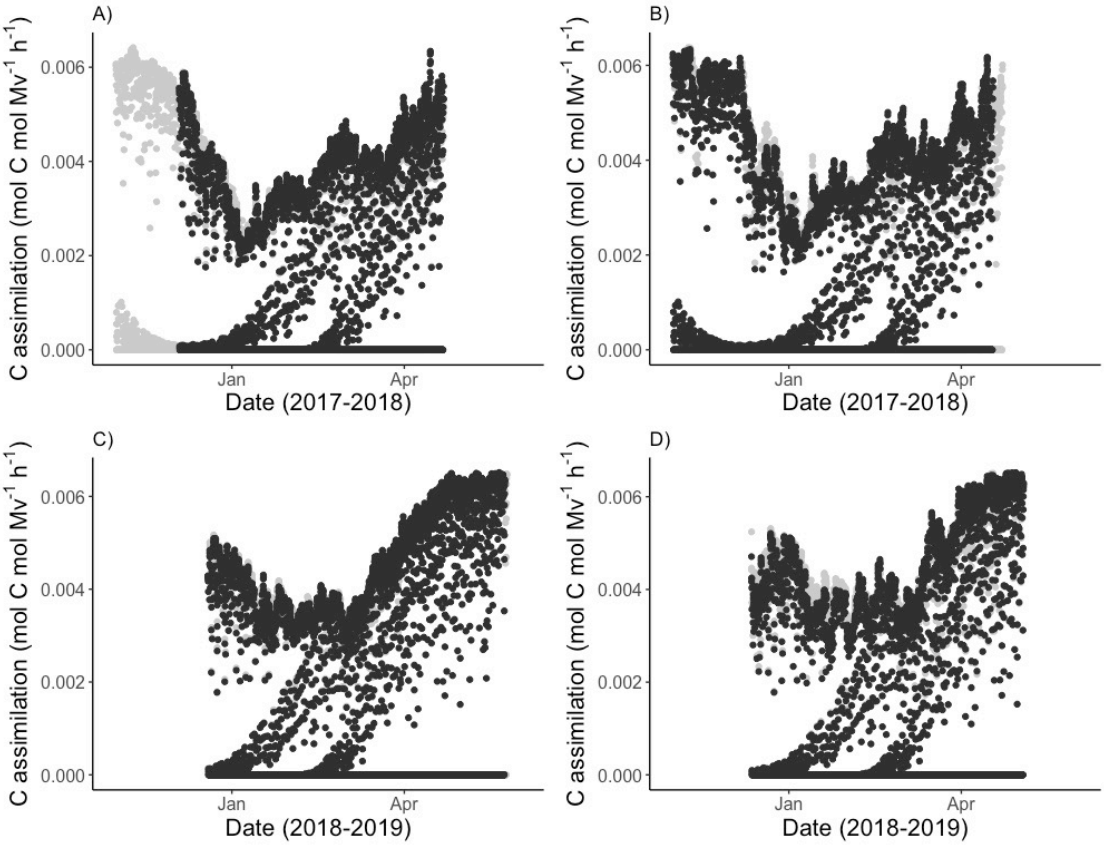

Figure S5d. Modeled carbon assimilation rates for kelp lines from the 2017-2018 growing season (top row) and the 2018-2019 growing season (bottom row). Darker grey is for the north lines and the lighter grey is for the south lines. A) and C) are Narragansett Bay N and S and B) and D) are Pt. Judith Pond N and S.